Universitetet
i Stavanger

FACULTY OF SCIENCE AND TECHNOLOGY

MASTER'S THESIS

Study programme/specialisation: **Petroleum Engineering /** **Natural Gas Engineering**	Spring semester, 2017 Open
Author: **Rashid Shaibu**	…… (signature of author)

Faculty Supervisor: **Jann Rune Ursin**

External Supervisor: **Yen Adams Sokama-Neuyam**

Title of master's thesis:

A Theoretical Study of The Effect of Salt Precipitation on CO_2 Injectivity

Credits: 30

Keywords: -Salt precipitation -CO_2 Injectivity -Saline Aquifer -Bundle of tubes -Carbon capture and storage	Pages: 83 Stavanger, 15th June, 2017

Dedication

I wish to dedicate this thesis work to the memory of my beloved aunty, Mariam, who has been very keen on my education but unfortunately passed away few months to the commencement of my masters studies.

Acknowledgement

I give thanks to the Almighty God for giving me the strength to complete this thesis work.

Special thanks to my supervisor Prof. Jann Rune Ursin for the opportunity given me to work on this topic.

I am grateful to Yen Adams Sokama-Neuyam, a PhD candidate for his technical guidance and advice throughout this work. I appreciate the support.

I am also grateful to Prof. Mrs Esi Awuah who has become my academic mentor and a mother and who also helped facilitate my study abroad.

To my parents and my uncle Sachibu, i ask for God's continuous blessings for them for their invaluable support, advice and encouragement.

Abstract

Global concern on climate change due to the greenhouse effect has led to various efforts to tackle anthropogenic Green House Gas (GHG) emissions. Of the various GHGs, CO_2 poses the greatest threat to the fight against climate change. Carbon Capture and Storage (CCS) especially in saline aquifers is recognized as a key solution to reducing atmospheric CO_2. Injectivity problems may however arise due to brine vaporization and consequently salt precipitation when dry super critical CO_2 is injected into saline aquifers. Several experimental and numerical studies have reported various levels of injectivity impairment attributed to salt precipitation but the mechanism of injectivity reduction is still uncertain. This work focused on the study of the basic mechanisms of salt distribution in the porous medium during precipitation and the consequences on CO_2 injectivity. A theoretical model to quantify injectivity loss due to salt precipitation was developed using a bundle of capillary tubes model. The model can reproduce some experimental results of drying of brine-saturated sandstone cores by supercritical CO_2 injection in the laboratory. A sensitivity of the parameters affecting injectivity show that; **(1)** salt precipitation occurs in the dry-out zone where most of the irreducible water in the trapped brine have evaporated, **(2)** increasing brine salinity has adverse effect on injectivity, **(3)** salt precipitation affects permeability more than porosity and **(4)** in rocks with high initial permeability, salt precipitation is minimal. These findings are important for a successful CCS project since CO_2 injectivity controls essential aspects of storage which are the rate, the quantity and length of time for CO_2 injection in a formation.

Contents

List of Figures

List of Tables

Abbreviations

CAPEX	Capital Expenditure.
CBM	Coal Bed Methane.
CCS	Carbon Capture and Storage.
CFCs	Chlorofluorocarbons.
EOR	Enhanced Oil Recovery.
GHG	Greenhouse Gas.
HS	High Salinity.
IEA	International Energy Agency.
IGCC	Integrated Gasification Combined Cycle.
IPPC	Intergovernmental Panel on Climate Change.
LS	Low Salinity.
NGO	Non-Governmental Organisation.
NIMBY	Not In My Back Yard.
OPEX	Operating Expenditure.
PDF	Probability Density Function.
PFBC	Pressurized Fluidized Bed Combustor.
PV	Pore Volume.
$scCO_2$	Super Critical CO_2.
SDGs	Sustenable Development Goals.
UNDP	United Nations Development Program.

Symbols

$\dot{m}$	Mass flowrate.
A	Crossectional area.
I_f	Final injectivity.
I_i	Initial injectivity.
L_{e1}	Lenght of dryout zone.
L_{e2}	Lenght of uncontaminated zone.
L_e	Total lenght of core.
N	Number of tubes.
P	Pressure.
Q	Volumetric flowrate.
R	Radius of core.
S_s	Solid salt saturation.
V_b	Bulk volume.
V_p	Pore volume.
V_s	Volume of precipitated salt.
X_s	Mass fraction of salt in brine.
Δr	Salt thickness.
α	Dryout coefficient.
β	Relative injectivity change.
μ	Dynamic viscosity.
$\overline{S_{g,d}}$	Average gas saturation.
ϕ	Porosity.
ρ_{aq}	Density of brine.
ρ_s	Density of salt.
σ	Standard deviation.
τ	Tortuosity factor.
k	Permeability.
m	non-logarithmic mean.
r_i	Radius of capillary tube.
v	Variance.

Chapter 1

Introduction

Since the industrial revolution, the world economy has been on a rapid growth and thrives on energy. The demand for energy therefore has also been on a high rise and consequently the use of fuels have increased, particularly fossil fuels. However, the abundant use of fossil fuels has raised worldwide concern due to their adverse effects on the environment particularly related to the emission of carbon dioxide (CO_2), a major anthropogenic greenhouse gas.

Increase in CO_2 concentrations in the earth's atmosphere enhances global warming and world leaders over the years have met on various forums to draft legislations geared towards decreasing CO_2 emissions. One of such recent meetings was in June 2017 on the Paris Climate Accord (2015) dealing with greenhouse gas emissions mitigation, adaptation and finance starting in the year 2020. The Paris Climate Accord also seeks to hold the global average temperature to well below 2 °C above pre-industrial levels and further take steps to limit the temperature increase to 1.5 °C above pre-industrial levels. Other such agreements are the Kyoto Protocol which was signed in 1997 and the UNDPs Sustainable Development Goals.

A part of mitigation methods to achieve global temperature increase below 2 °C is carbon capture and storage (CCS) in geological reservoirs. CCS is recognized as the best option for removing emitted CO_2 from the atmosphere although it comes with several challenges [36]. CCS includes the capture of CO_2 from point sources, transport to disposal sites, storage and monitoring. This is a costly technology and the various processes involved are still undergoing improvement for efficiency and cost effectiveness [34]. There are a few CCS projects in the world with many more coming on stream in the coming years whilst a lot more are still at the laboratory stage. Details with regards to the

various CCS stages and current projects are discussed under section 2.2 of this report. The screening of geological reservoirs for the storage of CO_2 depends on the storage capacity, injectivity and containment [36]. This work centres specifically on injectivity in order to understand the conditions that lead to its impairment. When talking about CO_2 injectivity, important aspects such as the quantity, the rate and length of time for injecting the CO_2 into a formation comes into the picture. These are fundamental for a successful CO_2 project and it becomes paramount to determine factors and in what way these factors influence CO_2 injectivity.

1.1 Problem Definition and Objectives

Deep saline aquifers are suggested as possible candidates for CO_2 storage based on storage capacity. However, injection of dry supercritical CO_2 into deep saline formations could vaporize brine near the well region and possibly precipitate salts, which might severely reduce CO_2 injectivity. Several experimental and numerical studies have reported various levels of injectivity impairment attributed to salt precipitation but the mechanism of injectivity reduction is still uncertain. The distribution of precipitated salt within the pore spaces is fundamental to understanding the mechanisms of injectivity impairment. Salt distribution in the dry-out zone depends on the concentration of salt in the brine, the petrophysical properties of the rock, CO_2 injection flow rate and the injection conditions. Understanding of these processes is essential for the long-term management of the evolution of CO_2 injection in geological formations.
The objectives of this research work are;

1. To develop a bundle-of-tubes model to study the basic mechanisms of salt distribution in the porous medium during precipitation and the consequences on CO_2 injectivity.

2. Perform sensitivity on the effect of various parameters on CO_2 injectivity.

Chapter 2

Theory

This chapter lays a foundation on which the proceeding chapters will be built on. In a chronological order, it reviews the various concepts relating to climate change and its mitigation—narrowing down to CCS. Various aspects of CCS which include sources of CO_2, its capture, transport and storage are discussed and a specific problem with storage, injectivity, which is the subject matter of this thesis is further discussed. The chapter completes with a description on pore scale modelling.

2.1 Climate Change and the Greenhouse Effect

Climate change is the change in the pattern of weather, and related changes in oceans, land surfaces and ice sheets—occurring over time scales of decades or longer [52]. Climate change is a manifestation of the greenhouse effect, which is caused by greenhouse gases in the atmosphere, trapping and redirecting heat back to Earth and causing global warming Figure 2.1.

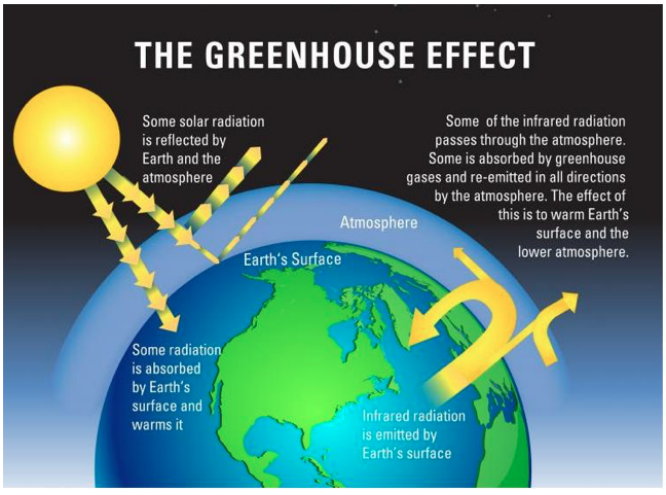

Figure 2.1: The Greenhouse Effect. [56]

Greenhouse gases have been shown in various studies to be the main contributor to the greenhouse effect and driver of global warming [55, 68]. While the existence of these gases in the atmosphere is vital in keeping the earth temperature habitable, unnatural rise in their atmospheric concentration can raise global average temperatures to alarming levels [62].

Gases that contribute to the greenhouse effect (Figure 2.2) include:

1. **Water vapour:** The main greenhouse gas in the atmosphere but importantly, it acts as a feedback to the climate. Water vapour increases as the earth's atmosphere warms, but so does the possibility of clouds and precipitation, making these some of the most important feedback mechanisms to the greenhouse effect [43] as depicted in Figure 2.3

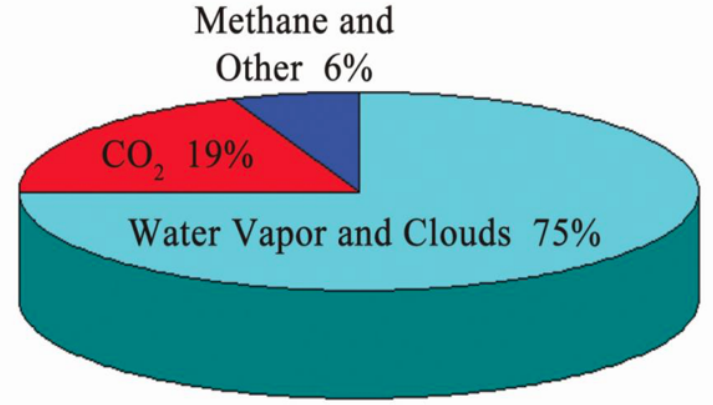

Figure 2.2: Contribution of various greenhouse gases to the greenhouse effect. [20]

2. **Carbon dioxide (CO_2):** The percentage of CO_2 in the atmosphere is relatively small but it is a very important component. It is identified as the main anthropogenic GHG, accounting for 80% of the human contribution to the greenhouse effect [21, 43]. It is released through natural processes such as respiration and volcanic eruptions and through human activities such as deforestation, land use changes, and burning fossil fuels.

3. **Methane(CH_4):** A hydrocarbon gas produced both through natural sources and human activities, including the decomposition of wastes in landfills, agriculture, and especially rice cultivation, as well as ruminant digestion and manure management associated with domestic livestock. It less abundant in the atmosphere but more active than CO_2.

4. **Nitrous oxide:** A powerful greenhouse gas produced by soil cultivation practices, especially the use of commercial and organic fertilizers, fossil fuel

combustion, nitric acid production, and biomass burning.

5. **Chlorofluorocarbons (CFCs):** These are the only greenhouse gases that do not occur naturally. They have been developed by man for industrial purposes but now largely regulated in production and release to the atmosphere by an international agreement for their extremely powerful ability to contribute to destruction of the ozone layer. They can stay in the atmosphere for thousands of years [43, 12].

Lacis et al. [32] did mention that carbon dioxide, methane, nitrous oxide and the fluorinated gases are all well-mixed gases in the atmosphere that do not react to changes in temperature and air pressure, so the levels of these gases are not affected by condensation. Water vapour on the other hand, is a highly active component of the climate system that responds rapidly to changes in conditions by either condensing into rain or snow, or evaporating to return to the atmosphere.

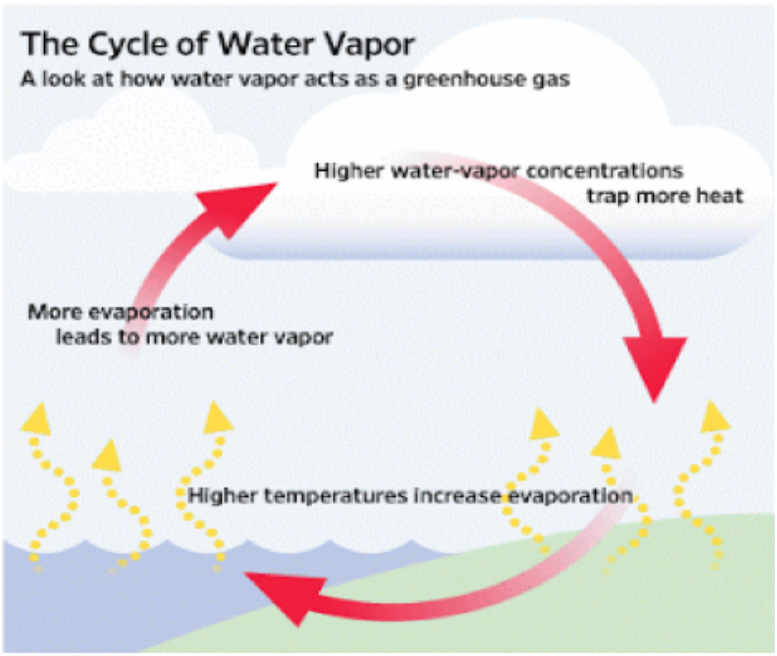

Figure 2.3: The water vapour feedback. [41]

Of all the greenhouse gases, excessive amount of CO_2 is particularly harmful because it can linger in the atmosphere for tens of thousands of years [2]. The CO_2 concentration in the atmosphere has increased rapidly since the industrial revolution, and achieved ca. 400 ppm. The concentration of CH_4 is 1.7 ppm and N_2O is 0.3 ppm. Hence their contribution to the greenhouse effect is less prominent than CO_2 [20, 40]. At present, human beings globally face serious energy and environmental issues. We have produced enormous energy with the use of fossil fuel accompanied with a significant development of industries. In a report

by the Intergovernmental Panel on Climate Change (IPPC) [35], it is stated that fossil fuels are the major cause of anthropogenic CO_2 emissions—contributing about three-quarters of all emissions through CO_2 generation by combustion process, exothermic chemical reactions involving (fossil) fuel to produce heat, manufacturing, transportation, and domestic activities.

The concern about global climate change have enhanced the attention on various approaches to minimize the CO_2 and other greenhouse gases [34]. These approaches can be largely put in three [40] broad categories which are:

(a) reducing the amount of CO_2 produced

(b) utilisation of CO_2

(c) capture and storage of CO_2 (CCS)

Some Governments have created regulations like carbon taxing and crafted laws aimed at minimizing CO_2 disposal to the atmosphere. However, these are not sustainable in the long-term. IPCC Working Group I as cited by Miri [36] has proposed a set of pathways to stabilize the atmospheric CO_2 concentration at 450, 550 and 750 ppmv over the next hundred years. Out of the several mitigation options, carbon capture and storage (CCS) in geological reservoirs is recognized as the best solution with respect to mitigation potential. CCS has the potential to reduce overall mitigation costs and increase flexibility in achieving greenhouse gas emission reductions [19]. Other mitigation options include energy efficiency improvements, the switch to less carbon-intensive fuels nuclear power, renewable energy sources, enhancement of biological sinks, and reduction of non-CO_2 greenhouse gas emissions [34, 43]. Table 2.1 compares the application areas, advantages and limitations of these different approaches.

2.2 Carbon Capture and Storage (CCS)

Carbon capture and storage (CCS) is an emerging technology which can reduce CO_2 concentrations in the atmosphere. Investigations by the International Energy Agency (IEA) have shown that CCS can contribute to 14% of the reduction in global greenhouse gas emissions required by 2050 (thus 50–85% from 2000 levels) to limit global warming to 2^oC [64] . However, it does not reduce fossil fuel dependency, and long-term CO_2 storage failities are not yet tested [66].

The main stages in the CCS process are: capture, transportation and storage.

Table 2.1: Summary of CO_2 reduction strategies [34]

Strategy	Application area/sector	Advantages	Limitations
Enhance energy efficiency and energy conservation	Commercial and industrial buildings	Energy saving from 10 % to 20 % easily achievable.	May involve extensive capital investment for installation of energy saving device.
Increase usage of clean fuels	Substitution of coal by natural gas for power generation.	Natural gas emits 10 % to 20 % less CO_2than coal due to its lower carbon content and higher combustion efficiency.	Higher fuel cost for conventional natural gas. Comparable cost for shale gas.
Adopt clean coal technologies	Integrated gasification combined cycle (IGCC), pressurized fluidized bed combustor (PFBC) etc.	Allow the use of coal with lower emissions of air pollutants.	Significant investment needed to roll out technologies widely.
Use of renewable energy	Hydro, solar (thermal), wind power, and biofuels highly developed.	Use of local natural resources; no or low greenhouse and toxic gas emissions.	Applicability may depend on local resources availability and cost. Power from solar, wind, marine etc. are intermittent and associated technologies are not mature.
Development of nuclear power	Nuclear fission adopted mainly in US, France, Japan, Russia and China. Nuclear fusion still in research and development phase.	No air pollutant and greenhouse gas emissions.	Usage is controversial; development of world's nuclear power is hindered due to the Fukushima Nuclear Accident in 2011, e.g. Germany will phase out all its nuclear power by 2022.
Afforestation and reforestation	Applicable to all countries	Simple approach to create natural and sustainable CO_2 sinks.	Restricts/prevents land use for other applications
Carbon capture and storage	Applicable to large CO_2 point emission sources.	It can reduce vast amount of CO_2 with capture efficiency 480 %.	CCS full chain technologies not proven at full commercial scale

There is also the need for monitoring, which should start before injection and continue after the storage site is capped and until stability of injected CO_2 is demonstrated [34]. As shown schematically on Figure 2.4, CO_2 is collected from large industrial sources, such as power stations, refineries or cement works, transported and then injected deep below the surface.

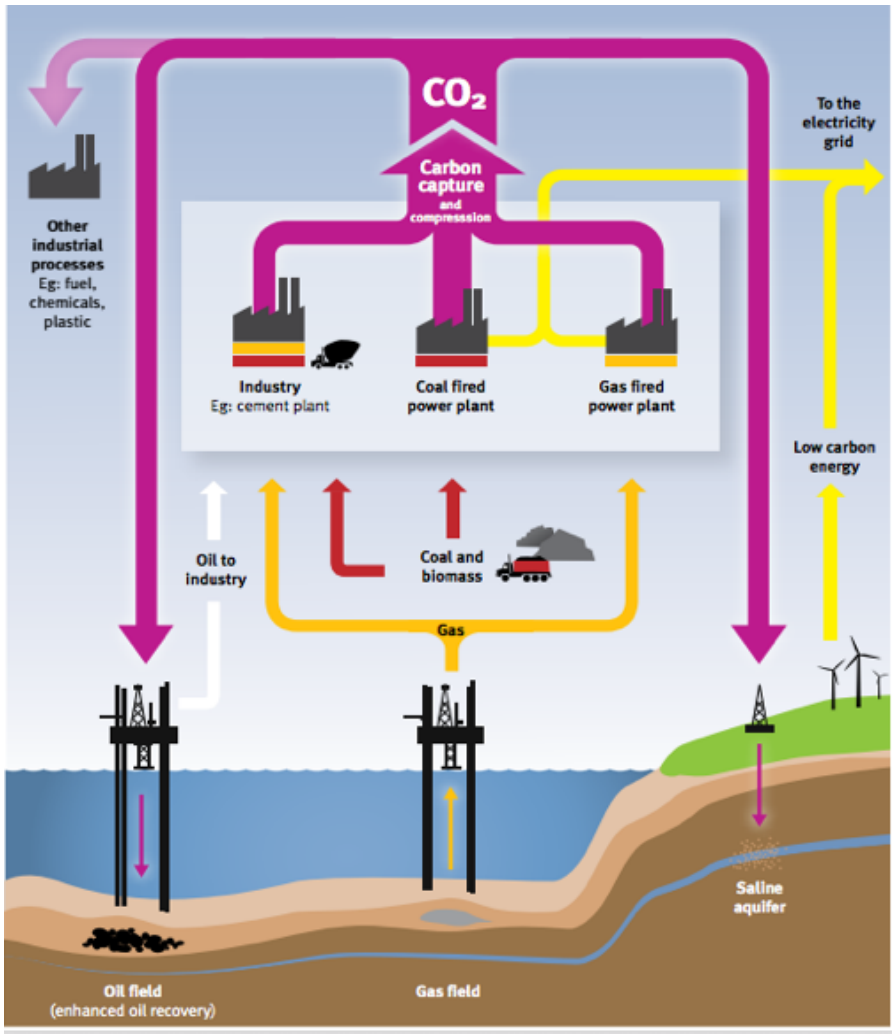

Figure 2.4: Schematic of carbon capture and storaget. [5]

2.2.1 Sources of CO_2

There are both natural and human sources of carbon dioxide emissions. Natural sources include decomposition, ocean release and respiration. Human sources come mainly from fossil fuel combustion in the power generation, industrial, residential and transport sectors [24]. Figure 2.5 shows the percentage emissions from these sectors. In the power generation and industrial sectors, many sources have large emission volumes that make them flexible for incoporating CO_2 capture technology. Large numbers of small point sources and mobile sources such as in

the case of transport, characterize sectors that are less amenable for capture at present. [35]

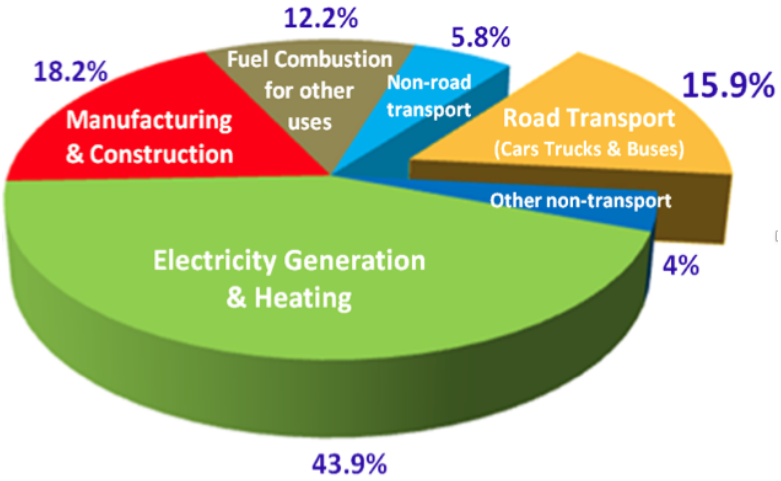

Figure 2.5: CO_2 emissions from fuel combustion.[9]

2.2.2 CO_2 Capture Technologies

Three main CO_2 capture techniques associated with different combustion processes, namely, post-combustion, pre-combustion and oxyfuel combustion are presently in use. These three technologies are shown in Figure 2.6 and discussed in the subsequent sections.

(a) **Post-combustion CO_2 capture:** this comprises the elimination of CO_2 from the flue gas produced by combustion. As shown in Figure 2.6, power plants use air, which has a high nitrogen fraction for combustion and generate a flue gas that is at atmospheric pressure. The adsorption process involves selectively scrubbing CO_2 from a gas stream using lean amine solvent. CO_2-rich amine and a CO_2-depleted gas stream results. The CO_2-rich amine is then further processed by the addition of heat, releasing a high purity CO_2 stream [19]. The concentration of CO_2 in the combustion flue gas is normally quite low—usually less than 15% (i.e. 7–14% for coal-fired and as low as 4% for gas-fired) [34]. Thus the thermodynamic driving force for CO_2 capture from flue gas is low (CO_2 partial pressure is typically less than 0.15atm), creating a technical challenge for the development of profitable innovative capture methods. Notwithstanding this difficulty, post-combustion carbon capture provides the best near-term potential for GHG emissions reduction because it can be retrofitted to existing units that generate two-thirds of the CO_2 emissions in the power sector [16].

(b) **Pre-combustion CO_2 Capture:** The pre-combustion process removes carbon from the source fuel before combustion [34, 16]. The fuel gas undergoes a gasification process conducted in a gasifier under low oxygen level to form synthesis gas (syngas) or fuel gas composed mainly of carbon monoxide (CO) and hydrogen H_2 [19]. The syngas will then undergo a water-gas shift reaction with steam forming more H_2 while the CO gas will be converted to CO_2. Finally, the H_2 is separated from the CO_2. The CO_2 can be compressed for transport and storage [35]. High temperature metals are required to withstand the temperatures reached when combusting H_2. This therefore require a more significant change to power plant or boiler design for pre-combustion processes. The capability of industrial equipment to combust H_2 thus becomes very important and could place a barrier to the implementation of pre-combustion technology. Much of the current research into pre-combustion technologies therefore focuses on improving the efficiency of the hydrogen production process. [19]

(c) **Oxyfuel combustion CO_2 Capture:** In oxyfuel combustion, nearly pure oxygen, instead of air, is used for combustion. This reduces the amount of nitrogen present in the exhaust gas that affects the subsequent separation process. CO_2 concentration of flue gas is increased significantly (80–98%) resulting in a simple and less expensive capture of CO_2 compared to post-combustion capture [19]. Substantial reduction in thermal NOx is another advantage of this process since nitrogen is never introduced into the combustion process [34]. However, the combustion of fuel in pure oxygen drives the combustion temperature above the limits of conventional metals and turbines [35]. Therefore, either specialized materials must be developed, or the temperature in the combustion chamber must be moderated. One method for moderating temperature is an O_2/CO_2 cycle. This involves the recycle of CO_2 from flue gas to the combustion chamber [19, 35]. Steam or water can also be used in place of CO_2 for moderating temperature. The resulting CO_2 can be compressed, transported and stored.

Comparing the three capture techniques, pre-combustion is mainly applied to coal-gasification plants, while post-combustion and oxyfuel combustion can be applied to both coal and gas fired plants. Post-combustion technology is currently the most mature process for CO_2 capture [4].

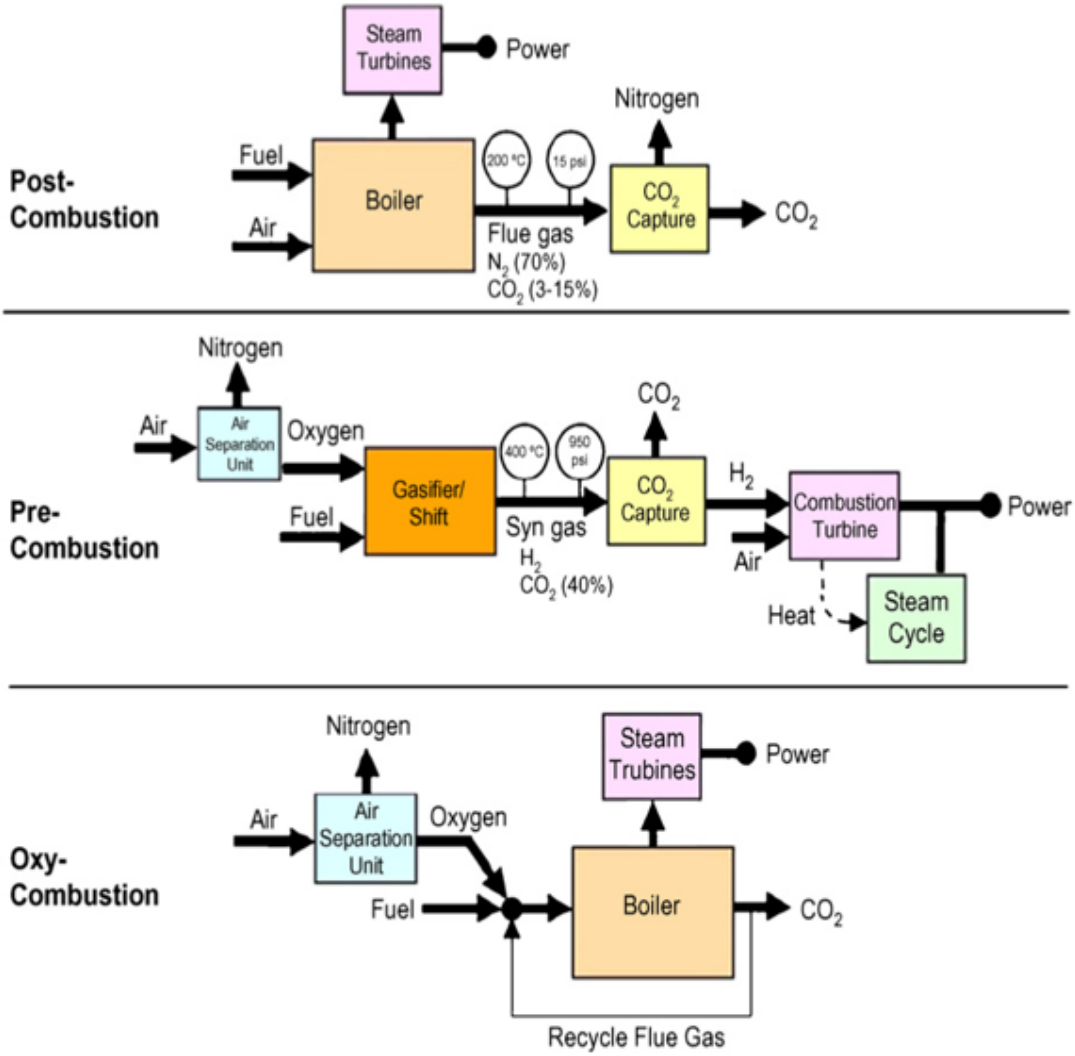

Figure 2.6: CO_2 capture methodologies. [16]

2.2.3 CO_2 Separation

Prior to transportation, the CO_2 needs to be isolated from the flue/fuel gas stream. Technologies used for this separation as stated by Leung et al. [34] include: absorption—using a liquid sorbent, adsorption—where a solid sorbent is used to bind the CO_2 onto its surface, hydrate based separation, cryogenic distillation, chemical looping combustion and membrane separation. Table 2.2 presents a comparison of the different separation techniques.

2.2.4 CO_2 Transport

After the separation of the CO_2 from the flue gas components, it either needs to be transported to a storage site or to facilities for its industrial utilization. A reliable, safe and economically sound system of transport is a key feature of any CCS project [34]. The most economic method of transport depends on the locations of capture and storage, and the quantities of CO_2 to be transported [44]. The main transport options ranges from road tankers to ships and pipelines

Table 2.2: Comparison of CO_2 capture technologies [34]

Capture Process	**Application Area**	**Advantages**	**Disavantages**
Post-combustion	Coal-fired and gas-fired plants	Technology more mature than other alternatives; can easily retrofit into existing plants;	Low CO_2concentration affects the capture efficiency.
Pre-combustion	Coal-gasification plants	High CO_2 concentration enhance sorption efficiency; fully developed technology, commercially deployed at the required scale in some industrial sectors; opportunity for retrofit to existing plant;	Temperature associated heat transfer problem and efficiency decay issues associated with the use of hydrogen-rich gas turbine fuel; high parasitic power requirement for sorbent regeneration;
Oxyfuel combustion	Coal-fired and gas-fired plants	Very high CO_2 concentration that enhances absorption efficiency; mature air separation technologies available; reduced volume of gas to be treated, hence required smaller boiler and other equipment;	High efficiency drop and energy penalty; cryogenic O_2 production is costly; corrosion problem may arise;
Chemical looping combustion	Coal-gasification plants	CO_2 is the main combustion product, which remains unmixed with N_2, thus avoiding energy intensive air separation;	Process is still under development and inadequate large scale operation experience;

[19]. Svensson et al. [61] pointed out that pipelines are the most viable method for both onshore and offshore transport of high volumes of CO_2 through long distances whereas ship tankers are mostly for offshore. Pipelines are also the most efficient way for CO_2 transport when the source of CO_2 is a power plant with a lifetime is longer than 23 years. For shorter period road and rail tankers are more competitive [44].

CO_2 is transported as a dense phase either in liquid or supercritical conditions. Supercritical is the ideal state for CO_2 carried by pipelines, which implies that the pipelines working temperature and pressure should be kept within the CO_2 supercritical envelope, i.e. above 32 °C and 72.9 atm [28]. According to Forbes et al. [17], to ensure a stable single-phase flow through the pipeline, the usual range of pressure and temperature for a CO_2 pipeline is between 85 and 150 bar, and between 13 °C and 44 °C . Along the pipeline, there will be drop in pressure resulting from the reduction of the hydraulic head. This is compensated for by adding recompression stations along the length of the pipeline. Larger diameter pipelines allow lower flow rates with smaller pressure drop and therefore a reduced number of recompression stations; on the other hand, larger pipelines are more expensive therefore a balancing of costs needs to be done [19].

2.2.5 CO_2 Storage

The most sustainable choice for the storage of the large quantities of CO_2 is by geological storage. It is at the moment considered the most effective way to reduce global warming and related climate change [8]. The three (3) geological formations generally considered for CO_2 storage are: unmineable coal beds, depleted oil and gas reservoirs, and saline aquifers. Studies have shown that deep ocean storage and mineral carbonation are feasible alternatives to geological storage but they all come with various degrees of limitations. Leung et al. [34] did state that, ocean storage will face environmental concerns such as ocean acidification and eutrophication which will likely limit its application. For now, only the geological storage is commonly applied, while the ocean storage and mineral carbonation are still in research phase.

The choice of geological formations for long-term storage will consider the formation stability, its storage capacity, the existence of a cap rock with good sealing capability and the number and integrity of existing well bores [19]. Other requirements such as distance from the source of CO_2 and economic aspects related to infrastructure and socio-political conditions were mentioned by Leung et al. [34]

The IPCC [35] indicated that the worldwide potential storage capacity in geological formations is likely to be at least 2,000 Gt CO_2. This is the technical potential, using a technology or practice that has already been demonstrated. The IPCC recognizes that there may be a much larger potential for geological storage in saline formations but the upper limits are uncertain due to lack of information and an agreed methodology. The relative capacity of different storage sites is given in Table 2.3.

Table 2.3: Capacity of potential CO_2 storage sites in the world [19]

Sequestration Option	**Worldwide Capacity for CO_2**
Oceans	1,000s Gt
Deep saline formations	100s - 10,000 Gt
Oil and gas reservoirs	100 - 1,000 Gt
Coal seams	10 - 100 Gt
Terrestrial ecosystems	10s Gt
World emissions of CO_2 for 2000	25 Gt

2.2.5.1 Depleted Oil and Gas Fields and EOR

According to the IPPC [35], depleted oil and gas fields have considerable appeal as storage locations for CO_2 for the following reasons:

1. The traps which housed the oil and gas originally, have demonstrated their integrity and safety as long as the seals were not damaged during oil or gas production

2. The exploitation of the oil and gas involved the extensive study and characterization of the geological structure and physical properties of the fluids.

3. Computer models have been developed in the oil and gas industry to predict the movement, displacement behaviour and trapping of hydrocarbons.

4. Existence of infrastructure and wells already in place may be used for handling CO_2 storage operations.

In instances where hydrocarbon production is still in progress, the CO_2 scheme can be adjusted to maximize oil or gas production, which then becomes an EOR technique. When the EOR is complete, the CO_2 is left in the reservoirs, and additional CO_2 can be added to fill up the storage capacity. Griffiths et al. [19]

noted that the total volume of CO_2 stored during EOR will be relatively small compared with other storage options, but it is beneficial because the revenue from the oil offsets some of the capture and storage costs.

2.2.5.2 Unmineable Coal Seams

In nature, coal seams also contain gases such as methane. The gas is held in pores on the surface of the coal and in fractures in the seams [54]. At the same pressure, CO_2 has an affinity to coal that is almost twice as high as that of methane found in the coal seams [35, 19, 54]. This then means that when CO_2 is pumped into coal seams, it replaces the methane gas that is held in the coal and becomes sequestered through sorption in the coal [19]. The IPPC [35] estimated that The volumetric ratio of adsorbable CO_2:CH_4 ranges from as low as one (1) for mature coals such as anthracite, to ten (10) or more for younger, immature coals such as lignite. The methane produced through the process can be piped and sold which can partly offset the cost involved in the injection process. One of the key decisive factors for the selection of coal seams as storage sites for CO_2 is the coal permeability. With increasing depth, Coal permeability decreases owing to the fact that the cleats close with increasing effective pressure [35]. Most CBM-producing wells in the world are however less than 1000 m deep

2.2.5.3 Saline Formations

Deep aquifers occurring between 700–1000 m below ground level often has high salinity formation brines [29]. These saline aquifers have no commercial value but can be used to store injected CO_2 captured from CCS process. Deep saline aquifers have the largest identified storage potential as presented in Table 2.3. Celia and Nordbotten [8] stated that the estimated storage capacity is sufficient to store emissions from large stationary sources for at least a century. The main features of CO_2 trapping mechanisms in saline aquifers as presented by Leung et al. [34] are;

1. **Hydrodynamic trapping:** undissolved CO_2 is trapped by overlying low-permeability caprock,
2. **Residual:** the CO_2 rises through water-saturated rock and displaces water from the pore space.
3. **Solubility:** CO_2 is dissolves in the formation brine water
4. **Mineral:** dissolved CO_2 reacts with Ca, Fe, or Mg based mineral to form carbonate precipitates.

These mechanisms lead to various processes within the formation of which the precipitation of salt is one such process. The precipitation of salt has been addressed in various literature and has been shown to potentially affect CO_2 injectivity. This is the central theme of this thesis work and will be expanded on in the subsequent chapters.

2.2.5.4 Ocean Storage

Deep ocean storage is a non-geological CO_2 storage method. The Oceans are the biggest natural CO_2 sinks, hence, deep ocean storage can present a potential sink for large amounts of anthropogenic CO_2 [34]). This approach however faces a lot of challenges—both legal and environmental, than the geological storage methods. The IPPC [35] noted that, injecting large amounts of CO_2 directly into the oceans may affect the seawater chemistry such as reducing its pH and causing ocean acidification, which may lead to disastrous consequences to the marine ecosystem [53]. The 1972 Convention on the Prevention of Marine Pollution by Dumping of Waters and Other Matters prohibits storage of CO_2in the water column, if it is considered an industrial waste.

2.2.5.5 Mineral Carbonation

Mineral carbonation technology, also a non-geological CO_2 storage method is based on the fact that CO_2 reacts with magnesium and calcium silicate to form stable carbonates. These carbonates do not incur any long-term liability or monitoring commitments. Mineral carbonation is a potentially attractive sequestration technology for the permanent and safe storage of CO_2. Key points with this technology as presented by Olajire [45] are:

1. mineral carbonation costs are too high compared to other sequestration costs.

2. technology offers the potential for long-term safe CO_2 storage.

3. mineral carbonation has zero monitoring requirements.

4. technology can be an economically acceptable commercial process if carbonation reaction kinetics can be improved upon.

The concept is still at the laboratory stage.

2.2.6 Monitoring Subsurface CO_2 Storage

The monitoring of stored CO_2 needs to be done before, during and after injection. These three (3) phases of monitoring are necessary to ensure that the CO_2 remains underground [19]. Monitoring can be used to ensure and document effective injection well controls and verify the quantity of injected CO_2 that has been stored [35]. With proper monitoring techniques, optimization of the efficiency of the storage projects is achieved. Other benefits of monitoring subsurface CO_2 storage are to detect leakage and provide an early warning of any seepage or leakage that might require mitigating action.

According to the IPPC special report on carbon dioxide capture and storage [35], monitoring requirements include, injection rates and pressures, monitoring subsurface distribution of CO_2, injection well integrity, local environmental effects, Long-term stewardship monitoring and verification of CO_2 injection and storage inventory.

A wide variety of monitoring techniques are available and the choice of a technique is largely dependent on the storage site. Leung et al. [34] categorized the various techniques into these broad areas;

1. **Geoelectrical methods:** these are based on the variation of resistivity caused by the presence of CO_2.

2. **Geochemical sampling:** this involves fluid sample collection from boreholes inside the storage area and observing the chemical variation induced by the injection of CO_2.

3. **Tracers:** co-injection of specific compounds together with CO_2 can generate a specific fingerprint of the stored CO_2. These tracers can be detected even in very small concentration (ppm) allowing an identification of any seepage from the reservoir

4. **Gravimetry methods:** Changes in underground density due to the injection of CO_2 can be detected by small perturbation in the local gravitational field; a loss in density is observed when CO_2 displaces denser brine inside the reservoir.

Other methods are temperature logs, remote sensing, atmospheric monitoring, soil gas and microbiology.

2.2.7 Current Projects

The engineered injection of CO_2 into subsurface geological formations was first undertaken in Texas, USA, in the early 1970s, as part of EOR projects and has been ongoing there and at many other locations ever since. In 1996, the worlds first large-scale storage project was initiated by Statoil and its partners at the Sleipner Gas Field in the North Sea [35]. Several other pilots and commercial projects for CO_2 storage have ever since been launched.

2.2.7.1 The Sleipner Project, North Sea

The Sleipner project is offshore and found in the North Sea. The project partners consist of Statoil (operator), ExxonMobil E&P Norway, Lotos E&P Norway AS and KUFPEC Norway AS. Using absorption chemical solvent-based process (Amine), CO_2 is stripped from natural gas produced from the Sleipner West field and stored in a deep saline aquifer located in the Utsira Sand formation at a rate of 1 Mt CO_2/ year [35]. The formation lies about 800-1000 m below the sea floor with a storage capacity in the order of $6.6 \times 10^8\,m^3$ [30]. Storage of the CO_2 is monitored by seismic time-lapse surveys and these surveys have shown that the cap rock is an effective seal that prevents CO_2 migration out of the storage formation. The sleipner project does not require transport as the injection is direct. A schematic on the injection process is shown in Figure 2.7

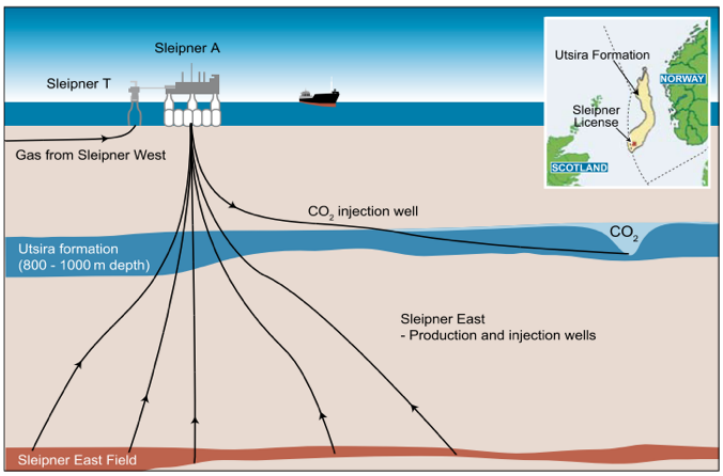

Figure 2.7: Sleipner CO_2 Storage Projects(simplified). [35]

2.2.7.2 The In Salah CO_2 Storage Project, Algeria

The In Salah CO_2 project, which includes capture, transport and storage was started in 2004 and it is expected to store about 17 Mt of CO_2 for the duration

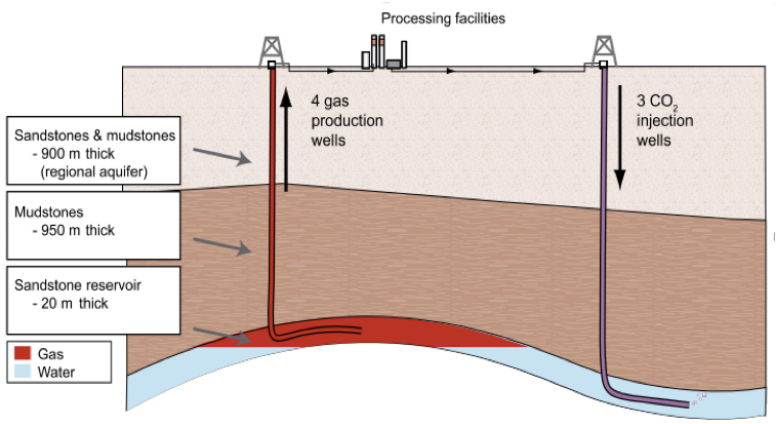

Figure 2.8: In Salah Gas Project (simplified). [35]

of its life IPPC. It is a joint venture among Sonatrach, BP and Statoil located in Algeria and is the worlds first large-scale CO_2 storage project in a gas reservoir [25]. Natural gas produced from the Krechba Field contains 10% CO_2. The gas is stripped off the CO_2 to meet commercial specifications. The captured CO_2 is then re-injected into a carboniferous sandstone at a depth of approximately 1,900 m / 6,200 ft below the surface and storing up to 1.2 Mt CO_2/year [25]. The Project in onshore and the mode of transport of the CO_2 is by pipeline of approximately 14 km. A schematic of the project is shown in Figure 2.8

Some upcoming CO_2 capture projects are presented in Table 2.4

Table 2.4: Upcoming geological storage projects [33]

Project Name	**Location**	**Operation Date**	**Capture Capacity (Mtpa)**
Sinopec Qilu Petrochemical CCS Project	China	2019	0.5
Rotterdam Opslag en Afvang Demonstratieproject (ROAD)	Netherlands	2019-20	1.1
CarbonNet Project	Australia	2020's	1.0-5.0
Lake Charles Methanol	USA	2021	4.2
Norway Full Chain CCS Project	Norway	2022	1.3

2.2.8 General CCS Challenges

CCS is a key part of worldwide efforts to combat global warming by reducing greenhouse gas emission to attain the IEA target of reducing global temperature by 2 °C by 2050 [34]. However, CCS does not reduce fossil fuel dependency and long-term CO_2 storage facilities are not yet tested [34, 66]. CCS still faces major backlash due to the unpredictability of the storage spaces and other environmental issues aside from the fact that the cost of the technology is expensive [60]. The challenges of CCS are varied and Zahra [70] put the various challenges into these four categories:

1. **Technical/industrial:** There are still uncertainties around CCS technologies with regards to performance, operation and scale up. Experience with large-scale geological storage, including the estimates of storage capacity in the various formations is limited [19]. The high costs and energy penalties involved also provides a major challenge for the deployment of CCS in large scale. With lots of research still ongoing for the development of novel capture and storage techniques, knowledge sharing is limited.

2. **Regulatory:** There is lack of appropriate legal and regulatory frameworks specifically dealing with CCS. According to the IPCC special report on carbon dioxide capture and storage [35], there are no regulations relating specifically to long-term responsibility for storage. Existing laws on offshore geological storage that existed before CCS may be relevant for CO_2 storage, however consideration of whether these laws do or do not permit offshore geological storage is under way.

3. **Financial:** CCS requires higher CAPEX and OPEX. The capture costs take about 75% of the CCS project costs—it ranges between 30 and 70 USD per tonne while the storage cost has been estimated to lie between 2–12 USD per tonne [34]. There is the need for technological developments to bring the costs down. The lack of financial resources to support projects of sufficiently large scale to evaluate the viability of CCS is a major challenge.

4. **Social Challenges:** As pointed out by Leung et al. [34], the success of deploying CCS technology will require meaningful public engagement on the subject. Members of the public are least informed on issues of CCS—they will usually take interest when projects are reviewed for licensing. A public survey by Wallquist et al. [67] on peoples preference for CCS showed that most people will not want to have any activity related to CCS anywhere close to their settlement be it transport or storage. the so called NIMBY

effect (Not in my backyard). Some are of the view that CO_2 is an explosive gas. Leung et al. [34] noted that when the public does show interest, it is likely that non-governmental organizations (NGO) will play a key role in determining the acceptance of this technology. Conflict of interest by the producers of subsidised electricity and ideological views, such as "by financing CCS, you cut financing for development of longer lasting solutions, such as renewable energies" have resulted in strong opposition to CCS development [26]. Massive public education is therefore paramount to inform the people of issues related to CCS especially concerning those on the environment.

2.3 Mechanisms of CO_2 Injectivity Impairment

Research has shown that saline aquifers could provide the largest sites for CO_2 disposal. CO_2 is injected in a supercritical state ($scCO_2$) that has a much lower density and viscosity than the liquid brine it displaces. However, injecting supercritical CO_2 into the saline formations leads to subsurface reactions such as CO_2 dissolution, pH variation of original brine and mineral dissolution/precipitation which collectively, can induce salt precipitation. Precipitated salt could modify the original porosity and permeability and affect injectivity [18, 1]. Experimental results of Muller et al. [39] showed a 60% permeability reduction due to halite precipitation in sandstone cores. Bacci et al. [3] also showed changes in porosity resulting from permeability variations during supercritical CO_2 core flooding experiments. Sustainable injectivity is important for a CO_2 sequestration. The reservoir injectivity—a key factor in deciding the feasibility of CO_2 storage in a candidate formation, measures the ability of a reservoir to accept CO_2 at maximum possible flow rate before losing its mechanical integrity. Any mechanism, negatively affecting injectivity therefore could have dire consequences on a CCS project [36].

2.3.1 Physics of Salt precipitation

Continuous injection of CO_2 in an initially saturated porous medium causes water displacement and evaporation. The injected CO_2 creates a two-phase flow regime and a drainage process is initiated. At the leading edge of the moving front, the CO_2 pushes out the formation water from the porous medium Figure 2.9a . The displacement of the water leaves pockets of trapped irreducible water in pores and films of water on the grain surfaces which is exposed to constant flowing dry CO_2 [36, 1, 71]. An extensive evaporation process begins and leads to the

development of a dry out front moving into the medium [1, 37]. Subsequently, salt precipitates out in the dry out region. Although the solubility of water in the scCO$_2$ is much smaller than the solubility of the CO$_2$ in the brine, substantial fraction of water will vaporize into the CO$_2$ stream causing the formation of the dry-out under constant flow of CO$_2$ [49, 59].

Miri and Hellevang [37] noted that the development of dry-out and level of precipitation are found to be consequences of interaction between several physical mechanisms which are:

1. Two-phase displacement of brine away from the injection well by viscous pressure gradients imposed through injected CO$_2$.
2. Evaporation of brine into the flowing CO$_2$ stream.
3. Capillary-driven back- flow of aqueous phase toward the injection point due to capillary pressure gradients
4. Molecular diffusion of dissolved salt in the aqueous phase,
5. Gravity override of injected CO$_2$
6. Salt self-enhancing.

Figure 2.9 shows schematically these mechanisms.

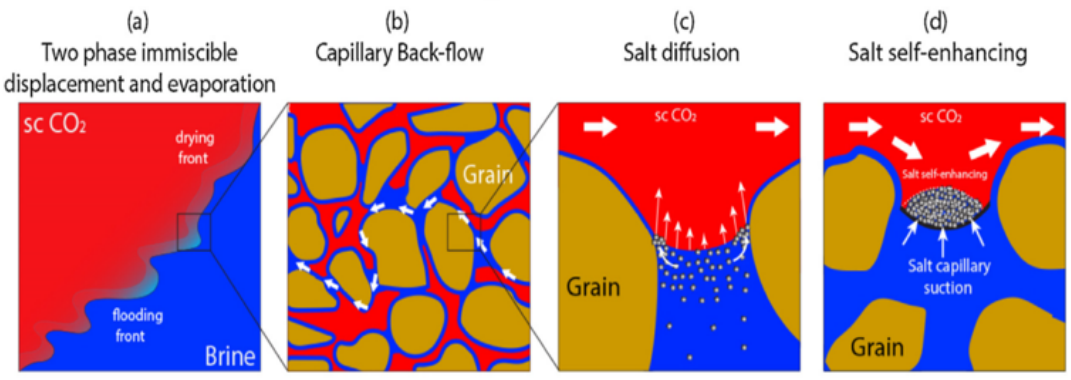

Figure 2.9: Physical mechanisms contributing to the process of salt precipitation. [37]

As evaporation and drying out occurs, the relative permeability of the CO$_2$ increases since the water saturation is being reduced. Increase in relative permeability of the CO$_2$ leads to more evaporation and as stated by Pruess [49], a dry-out front is formed which lags the displacement front. These two mechanisms, displacement and evaporation, contribute to water fraction being reduced in the

formation [36]. The two mechanisms however occur at different times. Little evaporation occurs during displacement and no convective flow during dry-out [37].

The water mass exchange in the dry-out zone creates a concentration gradient which decreases towards the displacement front [1, 36]. This is because the salt concentration in the dry-out zone becomes higher owing to the fact that, water has evaporated in this region. Once the salt concentration reaches its solubility limit owing to the evaporation, salt will precipitate out of solution [36]. The precipitated salt is then able to imbibe water from the flooding front and an effective capillary backflow is established (Figure 2.9b) once the capillary pressure gradient overcomes the injection pressure gradient [1, 47]. The water being drawn to the evaporation front leads to further evaporation and increase in salt concentration in the dry-out zone. Salt concentration in the trapped brine increases, resulting in salt diffusion Figure 2.9c towards the flooding front [37]. The relative distance between the dry-out front and the flooding front is largely controlled by this capillary backflow and solute diffusion. In addition, capillary flow due to salt Figure 2.9d is much stronger and gives significant stability to the water films, thereby enhancing salt precipitation [36].

2.3.2 Parameters Affecting Salt Precipitation

2.3.2.1 Salinity

Aquifer salinity is the single most influential parameter controlling salt precipitation [36, 72]. Pruess [49] showed through a series of experiments that reducing salinity by a factor 2 reduces solid saturation over proportionately by a factor of 2.23.

Increasing the brine salinity leads to more CO_2 remaining in the gaseous phase. This is because, the evaporation of water into CO_2 decreases which in turn reduces the dissolution of CO_2 in the brine significantly [72].
As presented in Figure 2.10 by Zeidouni et al. [72], the velocity of the leading shock increases because of the increase in CO_2 in the gaseous phase. On the same graph, increase in solid salt saturation owing to increase in salinity is demonstrated. Zeidouni et al. [72] explained that doubling the salinity causes roughly 8% increase in the velocity of CO_2 advancement into the aquifer.

Although higher brine salinity influences salt precipitation more, it has been shown to be dependent on flowrate [37, 63]. Low to intermediate permeability

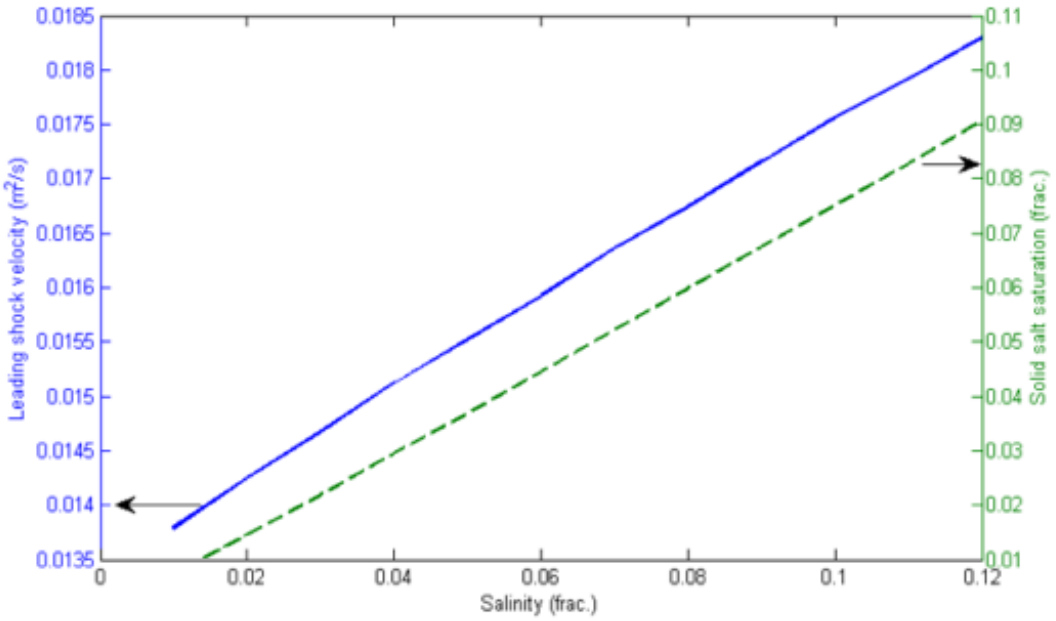

Figure 2.10: Leading shock velocity (solid curve) and solid salt saturation (dashed curve) versus salinity.[72]

reservoirs are most susceptible at low injection rates irrespective of formation water salinity [37]. However, for low salinity and high permeability reservoirs, field observations of injectivity impairment are yet to be reported [37].

2.3.2.2 Injection flowrate

Capillary backflow—which causes intensive salt precipitation (subsection 2.3.1) could be suppressed for high injection flowrates [28, 23]. An increase in the injection pressure will slow down the plume mobility owing to increased viscosity of the CO_2 phase, but further evaporation at higher injection pressures will increase the amount of precipitation—thus an increase in evaporation rate is more significant and can not be compensated for by a decrease in capillary back-flow with regards to salt accumulation [37].

2.3.2.3 Temperature

Generally, the effect of temperature on salt precipitation is insignificant [72]. Temperature may however vary since the injected CO_2 might have a different temperature than that in the aquifer. The effect of temperature on salt precipitation is affected by pressure as shown in Figure 2.11. Zeidouni et al. [72] explained that, this is mainly due to the different behaviour of vaporization on different pressure ranges. At higher pressures, the salt precipitation increases with temperature. However, at lower pressures, the precipitated salt saturation

declines to reach a minimum before it starts to increase with temperature [72].

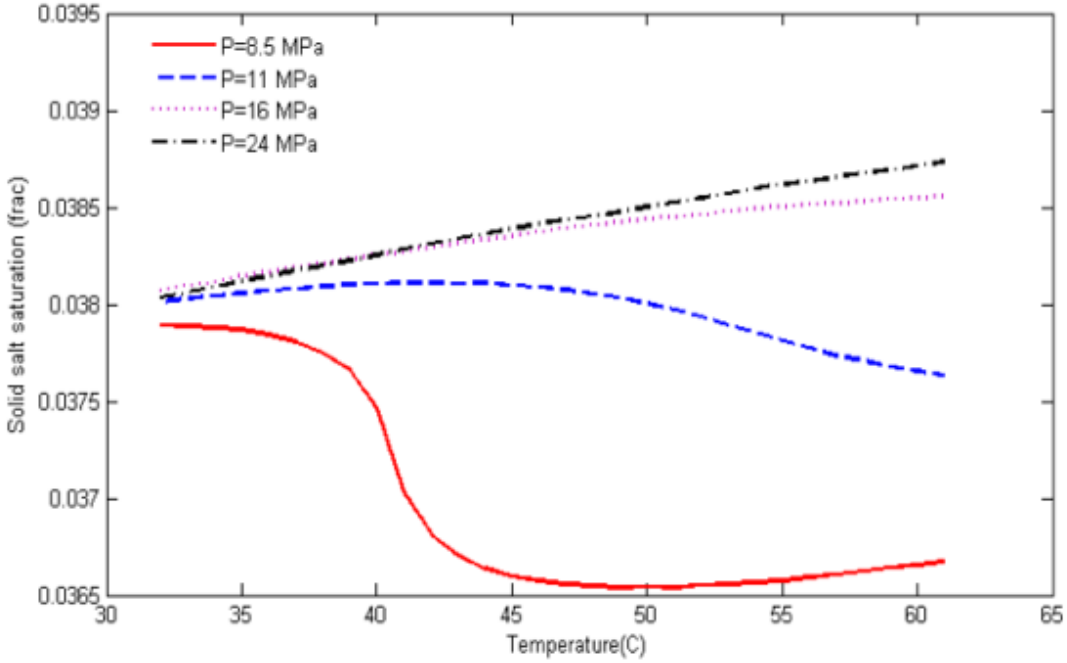

Figure 2.11: Solid salt saturation versus temperature for different pressures. [72]

2.3.2.4 Capillary Pressure

Capillary pressure will provide a driving force for drawing water toward regions with higher gas saturations, adding a flow component that opposes the generally outward flow, especially near the dry-out front where capillary pressure gradients are largest [49].

2.3.2.5 Effect of Aqueous and Gaseous Phases Relative Permeability

Zeidouni et al. [71] used an analytical model to investigate the effect of different parameters on both maximum CO_2 plume size and amount of salt precipitation. Their studies provided insight into the effects of relative permeability. An increase in relative permeability of the aqueous phase or decrease in the relative permeability of the gaseous phase, decreases both the amount of precipitated salt saturation and the extent of the CO_2 plume. Zeidouni et al. [71] concluded that, the salt precipitation is most affected by the brine salinity and aqueous phase relative permeability.

2.4 Pore-Scale Modelling

To be able to study the nature of fluid flow such as diffusion and dispersion flow in fractures, pore-scale evaporation processes etc., at the micrometre scale, network models are used [38]. There exist many of such models describing two-phase and three phase networks and flows. The suitability of the pore-scale modelling methods for a given purpose hangs on the governing equations, the fundamental assumptions for the pore-scale flow and transport equations, as well as the length-scales of the computational domain [69].
The construction of the various models which includes methods such as statistical reconstruction, grain based model and direct mapping usually require the geometry and topology of the pore space. The techniques commonly used to determine these include, imaging, mercury intrusion, porosimetry and gas adsorption [38, 69, 48]. The Pore network construction models have been explained extensively by Xiong et al. [69]

2.4.1 Existing models

The earliest use of the pore scale modelling was by Fatt et al. [13], who exploited the analogy between flow in porous media and a random resistor network. [5, 38]. Since then, various improvements and techniques have been used to develop models with good representation of the porous media. These models however are not perfect in general applications. They cannot make direct predictions of multiphase properties, but can be used to provide insight into flow in porous media and with proper tuning of parameters, they can be used to make predictions for conditions outside the range of their applicability [15].

Soll and Celia [58] simulated capillary pressure-saturation relationship at the pore level using a computationally developed model. They made use of percolation and network theories to describe fluid movement within the pore space in the computational approach. The porous medium was represented by two or three network of pores which were interconnected by throats. Unlike other models, every pore could accommodate one fluid at a time as well as wetting layers.

Fenwick and Blunt [14] developed a model for three-phase flow in a water-wet porous media. The model was composed of a cubic network comprising pores and throats with equilateral triangular or square cross-sections. The model could simulate any sequence of oil, water and gas injection.

Heiba et al. [22] extended the statistical network model and percolation theory of capillary pressure and relative permeabilities to three fluid phases (gas, oil and water). They used a Bethe lattice to represent the porous medium. They assumed for all cases that, gas is non-wetting relative to oil and water, and oil is non-wetting relative to water for convenience sake. Six groups of displacements were considered 1) gas into oil, 2) oil into gas, 3) gas into water, 4) water into gas, 5) water into oil, and 6) oil into water [48]. Two displacements were however studied. In one case gas and water were displacing oil while in the second case water and oil were displacing oil and gas. The results showed that the gas and water relative permeabilities were functions of only their own saturations [48].

Or and Tuller [46] simulated soil pores as a bundle of capillary tubes of different diameters and studied flow in unsaturated fractured porous media. Although the capillary model is widely used and is easy to obtain, it has a few shortcomings, primarily the over simplistic assumption regarding the binary nature of the pores (i.e., each pore is either completely water-filled or completely empty). Moreover, the lack of pores connectivity and the unrealistic cylindrical geometry of the capillaries further reduce the model efficiency in determining soil hydraulic properties

A simple capillary theory by Kozeny, in which the porous medium is envisaged as a bundle of parrellel capillary tubes (Figure 2.12) has been adopted in various porous media studies [31]. Verma and Pruess [65] used this idea where a porous medium is conceptualized as a series of connected tubes of varying sizes [37].

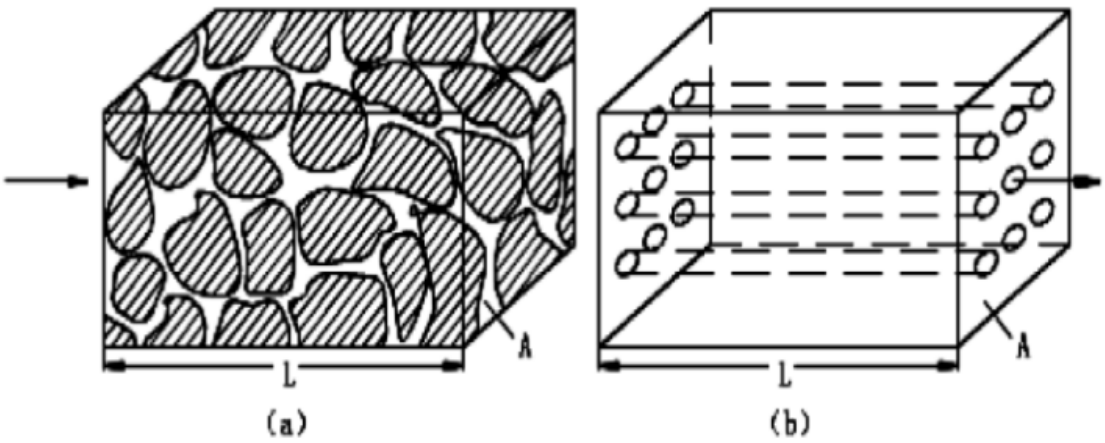

Figure 2.12: Porous media as a bundle of capillary tubes. [11]

The Capillary model is widely used and is easy to obtain. However, it has a few shortcomings; the lack of pores connectivity and the idealistic cylindrical geometry

of the capillaries reduce the model efficiency [48].
In this work, we adopt the capillary tubes model mainly for its simplicity and flexibility. We however incorporated tortuosity into the model to make it a bit realistic. An analytical model for tutoursity coefficeient derived by Jian-Hua and Bo-Ming [27] which was based on flow through the Sierpinski carpet is used.

Chapter 3

Model Development

3.1 Overview

This chapter presents the development of a model to study the basic mechanisms of salt distribution in a porous medium during precipitation and the consequences on CO_2 injectivity. A bundle of parallel tubes is used in the modelling where the effects of tortuosity have also been investigated.

3.2 The Bundle of Tubes Model

A bundle of tubes model is a model wherein the pore space of a porous medium is represented by a set of parallel capillary tubes [10] as shown in Figure 3.1. The white-dotted area is the rock matrix and the white-plain area is the capillary tubes representing the pore space. a typical porous medium, flow pathways are tortuous. If we assume that the tubes presented in Figure 3.1 are tortuous, and runs from the inlet of the core to the outlet as presented in Figure 3.2, a tortuosity factor τ, which is defined is defined as the ratio of the actual tube length L_e to the length of the cylindrical core L, can be written as:

$$\tau = \frac{L_e}{L} \tag{3.1}$$

where,

$$L_e = L_{e1} + L_{e2} \tag{3.2}$$

Assuming the porous medium could be sectioned into two distinct parts after salt precipitation; the dry-out zone L_{e1} and the uncontaminated zone L_{e2}. The cylindrical core with radius, R and length, L is represented by a bundle of parallel capillary tubes of varying radii $r_1, r_2, r_3, \ldots r_n$ interspersed in a non-porous mass.

Δr is the thickness of precipitated salt in the dry-out zone. It is shown as the thick black lines within the core.

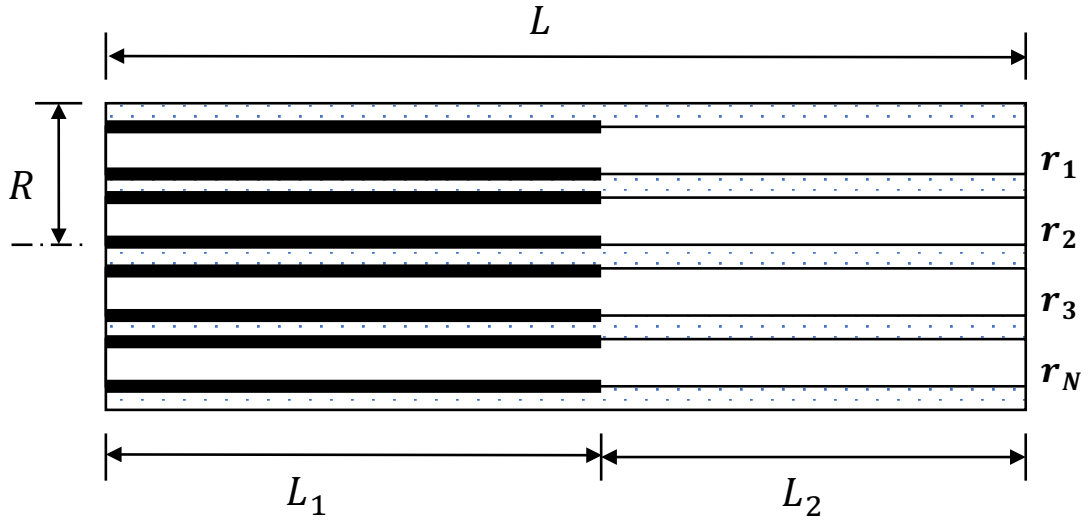

Figure 3.1: A bundle of tubes.

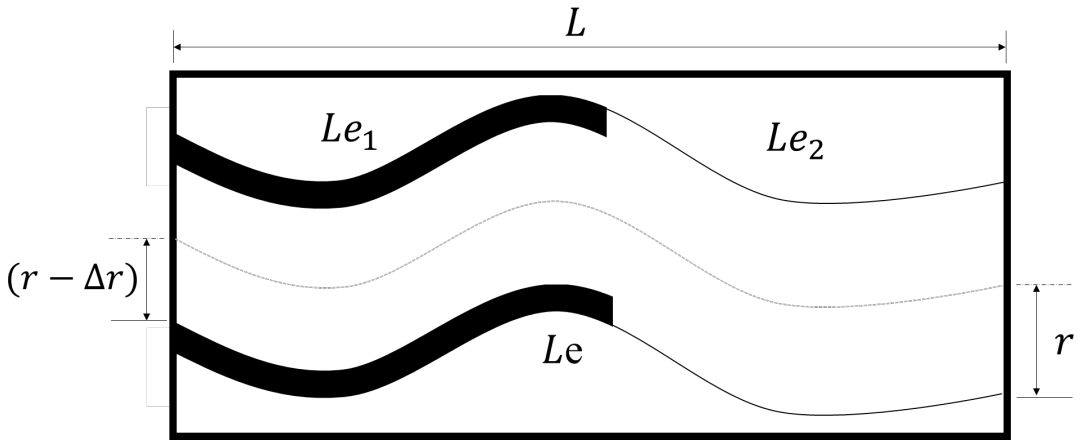

Figure 3.2: A single tortuous tube.

A dry-out coefficient, α, defined as the ratio of the length of the dry-out zone to the total length of the tortuous path is used to track the development of the dry-out zone.

$$\alpha = \frac{L_{e1}}{L} \tag{3.3}$$

Combining equations 3.1, 3.2 and 3.3, L_e and α, can be further expressed as:

$$L_e = \tau L \tag{3.4}$$

$$\alpha = \frac{L_e}{\tau L} \tag{3.5}$$

From equation 3.5, L_{e1} can be written as:

$$L_{e1} = \alpha\tau L \tag{3.6}$$

Combining equations 3.2, 3.4 and 3.5, L_{e1} can be expressed as:

$$L_{e2} = L_e - L_{e1} = \tau L(1-\alpha) \tag{3.7}$$

With equations 3.6 and 3.7, we can calculate the length of the dry-out zone and uncontaminated zone in terms of α, τ and L.

3.2.1 Estimation of the Tortuosity Factor, τ

The tortuosity factor was estimated using an already established analytical correlation of Jian-Hua and Bo-Ming [27] which was derived based on flow through the Sierpinski carpet. The only input parameter required for this model is porosity. The model is as shown in equation 3.8

$$\tau = \left(\frac{19}{18}\right)^{ln(\phi)/ln(8/9)} \tag{3.8}$$

The choice of this model is because of its simplicity and the absence of an empirical constant.

3.3 CO_2 Injectivity Quantification

Being able to quantify the injectivity of CO_2 into a core sample will give us the basis on which to study the mechanisms and physics surrounding salt precipitation and most importantly the effects of precipitation.

3.3.1 Flow Through a Single Tube

Assuming the dry-out region and the uncontaminated region are represented by two separated tortuous tubes (Figure 3.2), joined in series, the net pressure drop across the entire length of the tube can be expressed as:

$$\Delta P = \Delta P_1 + \Delta P_2 \tag{3.9}$$

Where ΔP_1 and ΔP_2 are the pressure drop across the dry-out region and the uncontaminated region respectively.

We used the poisseulles law to compute the pressure drops in equation 3.9. The Law states that the flow (Q) of fluid through a cylindrical tube of constant cross section is related to several factors; the dynamic viscosity(μ) of the fluid, the pressure gradient across the tubing (P), and the length (L) and radius (R) of the tubing. The law assumes incompressible and Newtonian fluid and larminar flow. The equation is written as:

$$Q = \frac{\pi R^4 \Delta P}{8\mu L} \tag{3.10}$$

Using 3.2 and 3.10, ΔP_1 and ΔP_2 can be computed as;

$$\Delta P_1 = \frac{8q_1\mu L_{e1}}{\pi(r-\Delta r)^4} \qquad = \frac{8q_1\mu\alpha\tau L}{\pi(r-\Delta r)^4} \tag{3.11}$$

$$\Delta P_2 = \frac{8q_2\mu L_{e2}}{\pi r^4} \qquad = \frac{8q_1\mu\alpha\tau L\,(1-\alpha)}{\pi(r-\Delta r)^4} \tag{3.12}$$

Where q_1 and q_2 are the fluid flow rate across the dry-out and uncontaminated region respectively. For the ΔP_1 (3.11), the radius of the tube is reduced by Δr due to salt precipitation.

On the field scale, the modelling of the processes leading to pressure drop becomes complex. Pressure drop in the formation is affected by potential energy, kinetic energy and frictional contribution to the overall pressure drop. The compressibility of the fluid need to be considered. When the fluid is compressible, its density and velocity vary within the formation and becomes important. However, for simplicity, we go with poisseulles law with its simplifying assumptions.

Assuming constant mass flow within the tubes (conservation of mass), the continuity equation, which states that the rate at which mass enters a system is equal to the rate at which mass leaves the system plus accumulation of mass within the system, can be written as;

$$\Delta\dot{m} = \rho_1 u_1 A_1 - \rho_2 u_2 A_2 = 0 \tag{3.13}$$

where $\dot{m}$ is the change in mass flowrate. We have assumed no accumulation of mass within the system. For incompressible flow, $\rho_1 = \rho_2 = \rho$. Equation 3.13 then reduces to equation 3.14, which is the volumetric flow rate, q;

$$q = u_1 A_1 = u_2 A_2 \tag{3.14}$$

therefore:

$$q = q_1 = q_2 \tag{3.15}$$

where μ is fluid velocity, and A is the cross-sectional area for fluid flow. Since

we assumed fluid incompressibility, the different velocities, u_1 and u_2 is because of change in cross sectional area from A_1 in the the dryout zone to A_2 in the uncontaminated zone.

Combining equations 3.9, 3.11, 3.12 3.15, the pressure drop across the single tube can be expressed as:

$$\Delta P = \frac{8q_1\mu\alpha\tau L}{\pi(r-\Delta r)^4} + \frac{8q_1\mu\alpha\tau L\,(1-\alpha)}{\pi(r-\Delta r)^4} \qquad = \frac{8q\mu\tau L}{\pi}\left(\frac{\alpha}{(r-\Delta r)^4} + \frac{1-\alpha}{r^4}\right) \tag{3.16}$$

3.3.2 Fluid Flow Through a Bundle Tubes

Modelling the cylindrical core of radius R in Figure 3.1 as a bundle of tortuous capillary tubes, the fluid flow rate through the core is the sum the total of the flow rate through each tube i;

$$Q = q_1 + q_2 + q_3 + ... + q_N = \sum_{i}^{N} q_i \tag{3.17}$$

where $i = 1, 2, 3, ...N$.
The pressure drop across the core is the same as pressure drop across each tube.

$$\Delta P = \Delta P_1 = \Delta P_2 = ... = \Delta P_N \tag{3.18}$$

combining equations 3.16, 3.17 and 3.18, the total flow rate can be expressed as:

$$Q = \frac{\pi\Delta P}{8\mu\tau L}\sum_{i=1}^{N}\left[\frac{1}{\frac{\alpha}{(r_i-\Delta r_i)^4} + \frac{1-\alpha}{r_i^4}}\right] \tag{3.19}$$

3.3.3 Estimating Injectivity Impairment Induced by Salt Precipitation

Fluid injectivity is defined as the ratio of the injection flow rate to the pressure drop. It is a measure of the potential of a well to inject fluid into a formation. It is written as;

$$I = \frac{Q}{\Delta P} \tag{3.20}$$

combining equations (19) and (20), the fluid injectivity can be expressed as

$$I = \frac{\pi}{8\mu\tau L}\sum_{i=1}^{N}\left[\frac{1}{\frac{\alpha}{(r_i-\Delta r_i)^4}+\frac{1-\alpha}{r_i^4}}\right] \tag{3.21}$$

In order the quantify the effect of salt precipitation on CO_2 injectivity, we introduce the relative injectivity change index, β;

$$\beta = \frac{I_i - I_f}{I_i} = 1 - \frac{I_f}{I_i} \tag{3.22}$$

where I_i is the initial injectivity, thus injectivity before the precipitation of salt. Before salt precipitation, the tube radii remain constant, and the dry-out region is assumed not to have appeared. Therefore $\Delta r = 0$ and $\alpha = 0$. Equation 3.21 will then reduce to:

$$I = \frac{\pi}{8\mu\tau L}\sum_{i=1}^{N} r_i^4 \tag{3.23}$$

I_f is the injectivity after salt precipitation and it is the same as equation 3.21;

$$I_f = \frac{\pi}{8\mu\tau L}\sum_{i=1}^{N}\left[\frac{1}{\frac{\alpha}{(r_i-\Delta r_i)^4}+\frac{1-\alpha}{r_i^4}}\right] \tag{3.24}$$

substituting equations (23) and (24) into (22) would yield;

$$\beta = 1 - \frac{\sum_{i=1}^{N}\left[\frac{1}{\frac{\alpha}{(r_i-\Delta r_i)^4}+\frac{1-\alpha}{r_i^4}}\right]}{\sum_{i=1}^{N} r_i^4} \tag{3.25}$$

The above equation will be solved over N radii to quantify the injectivity reduction. From the equation, there are three unknowns to be determined in order solve for β. These are $N, \Delta r$ and α.

3.3.4 Estimation of Total Number of Capillary Tubes, N

This is approached using the mathematical definition of porosity. Porosity can be simply defined as ratio of the pore volume V_p to the bulk volume V_b.

$$\phi = \frac{V_p}{V_b} \tag{3.26}$$

The total pore volume of the core will be the sum of internal pore volume of all the tubes.

$$V_p = \pi L_e \sum_{i=1}^{N} r_i^2 \quad \approx \pi \tau L N \overline{r_i^2} \tag{3.27}$$

$\overline{r_i^2}$= **average value of the square of tube radii**. The Bulk volume of core can be written as;

$$V_b = \pi R^2 L \tag{3.28}$$

substituting equations 3.27 and 3.28 into 3.26 yields;

$$N = \phi \frac{R^2}{\tau \overline{r_i^2}} \tag{3.29}$$

estimating the average value of the square of tube radii, $\overline{r_i^2}$ will be challenging but by integration we can show that;

$$\overline{r_i^2} = \frac{1}{\Delta r_{max}} \int_0^{\Delta r_{max}} r_i^2 dr_i \tag{3.30}$$

solving equation 3.30 yields;

$$\overline{r_i^2} = \frac{4}{3} \overline{r_i}^2 \tag{3.31}$$

where $\overline{r_i}^2$ is the **square of the average tube radii**, which is much easier to calculate. For this study, the average pore radius of a Berea sandstone is used. Substituting equation 3.31 into 3.28, the total number of tubes, N, in the core can be expressed as;

$$N = \frac{3\phi}{4\tau} \left(\frac{R}{\overline{r_i}} \right)^2 \tag{3.32}$$

3.3.5 Thickness of Precipitated Salt, Δr

The solid salt saturation in a single tube is defined by;

$$S_{si} = \frac{V_{si}}{V_{pi}} \tag{3.33}$$

where V_{si} is the volume of the precipitated salt in a single tube and V_{pi} is the pore volume of a single tube.

$$V_{pi} = \pi \tau L r_i^2 \tag{3.34}$$

From equation 3.20, the volume of the precipitated salt (volume of the shaded area) could be estimated as;

$$V_{si} = \pi r_1^2 \alpha\tau L - \pi\alpha\tau L\left(r_i - \Delta r_i\right)^2 \qquad = \pi\alpha\tau L\left(2r_i\Delta r_i - \Delta r_i^2\right) \tag{3.35}$$

where $\alpha\tau L = L_{e1}$ as shown in equation 3.6.
The thickness of the precipitated salt is expected to be very small, typically within the range of 10^{-7} to 10^{-9}. Assuming Δr is so small and that Δr_i^2 and other higher powers of Δr_i can be neglected, thus $\Delta r_i^2 \approx 0$, equation 3.35 reduces to;

$$V_{si} = 2\pi\alpha\tau L r_i \Delta r_i \tag{3.36}$$

by substituting equations 3.34 and 3.35 into 3.33, we get;

$$S_{si} = \frac{2\pi\alpha\tau L r_i \Delta r_i}{\pi\tau L r_i^2} = \frac{2\alpha\Delta r_i}{r_i} \tag{3.37}$$

It follows that the thickness of the precipitated salt could be expressed as;

$$\Delta r_i = \frac{S_{si} r_i}{2\alpha} \tag{3.38}$$

The mass of precipitated salt in a tube m_{si} could be estimated from the density of the salt, ρ_s and its volume in the tube as;

$$m_{si} = \rho_s V_{si} = 2\rho_s \pi\alpha\tau L r_i \Delta r_i \tag{3.39}$$

The total mass of solid salt precipitated in all N tubes, could then be estimated as;

$$m_t = \sum_{i=1}^{N} m_{si} = N\overline{m_{si}} \tag{3.40}$$

the Total mass of the precipitated salt can also be expressed as;

$$m_t = \rho_s V_{st} \tag{3.41}$$

where V_{st} is the total volume of precipitated salt in the porous medium. From equation 3.33, we can write V_{st} as a function of total solid salt saturation, S_s;

$$V_{st} = S_s \pi R^2 L\phi \tag{3.42}$$

substituting equations 3.32, 3.39, 3.41 and 3.42 into 3.40, the average thickness of precipitated salt in each tube could be expressed in terms of the total precipitated salt as;

$$\overline{\Delta r_i} = \frac{2S_s\overline{r_i}}{3\alpha} \tag{3.43}$$

Equations for the estimation of the three unknowns have now been established. However, equation 3.43 has an extra parameter that needs to be determined, which is the solid salt saturation (S_s).

3.3.6 Estimation of Solid Salt Saturation

Pruess [49] derived an analytical expression for the estimation of the solid salt saturation using properties of the fluids and the characteristics of the displacement process. He considered mass balance between injected CO_2stream and displaced brine and also adopted the fractional flow theory from Buckley, Leverett, et al. [7] to arrive at the expression given below;

$$S_s = \left(1 - \overline{S_{g,d}}\right) \frac{\rho_{aq} X_s}{\rho_s} \tag{3.44}$$

In equation 3.44 $\overline{S_{g,d}}$ is the average gas saturation in the dry-out zone, ρ_{aq} is the density of brine, X_s is the mass fraction of salt in the brine and ρ_s is the density of solid salt. α is substituted into equation 3.44 for $\overline{S_{g,d}}$ since they both in a way tracks the development of the dry-out zone. A correlation for solid salt saturation was derived (3.45), by fitting experimental data.

$$S_s = (0.85 + 0.1\alpha) \frac{\rho_{aq}}{\rho_s} \tag{3.45}$$

Obtaining the experimental data was done prior to the commencement of this study. First, ρ_{aq} and X_s were measured for a 100 g/l NaCl brine. Then, a Berea sandstone core-sample with known initial permeability, was saturated with the brine and about 300 PV of supercritical $CO_2$was flooded through the core at a rate of 5 ml/min. After every 100 PV of CO_2 injections, the core was inspected to determine α after which permeability was measured. The saturation correlation is optimized to fit the experimental data. The optimum correlation in equation 3.45 is used throughout this work.

3.4 Computational Algorithm

Figure 3.3 shows schematically the procedure involved in computing for the value of the relative injectivity index, β. The initial injectivity is first calculated using input parameters, α, $\overline{r_i}$ and N after which the solid salt saturation is calculated using Equation 3.45. The thickness of the salt is calcuated from the solid salt saturation, α, and $\overline{r_i}$. The final inejctivity I_f which depends on the salt thicknes is then computed and with Equation 3.25 the relative injectivity change is determined.

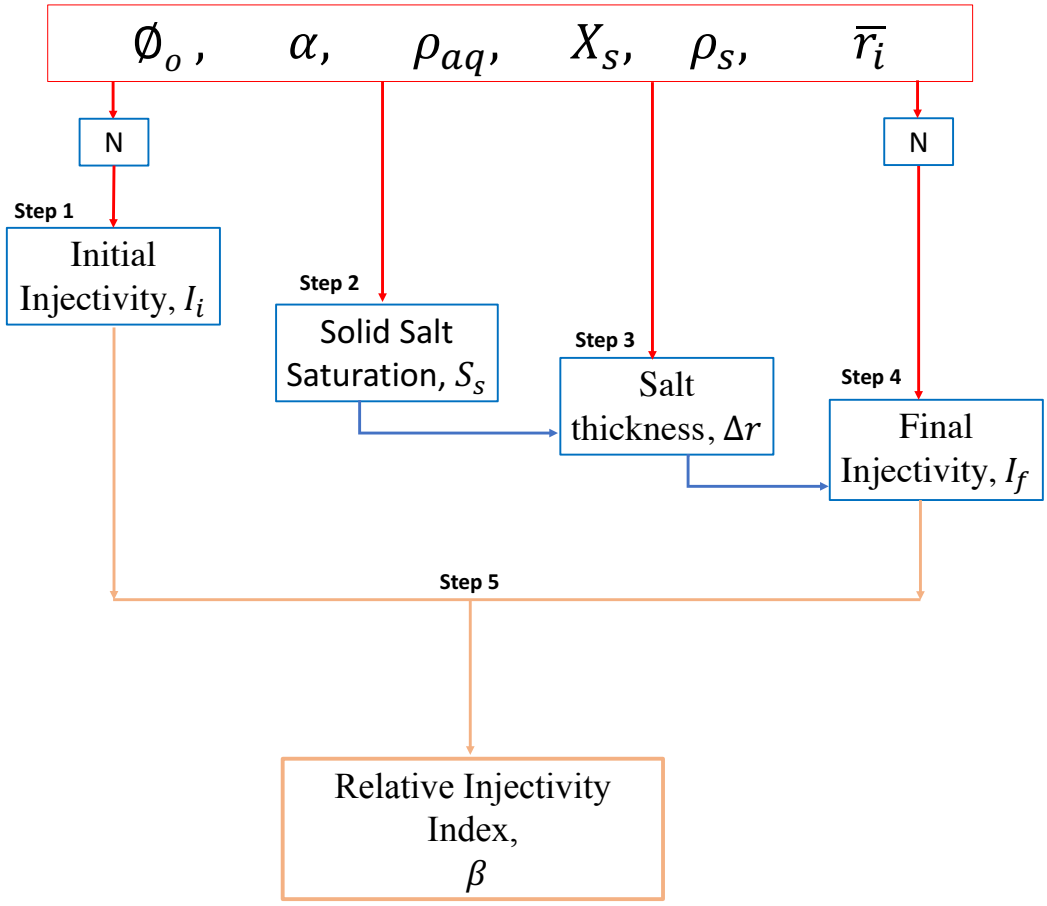

Figure 3.3: Control algorithm

Chapter 4

Results and Discussion

4.1 Overview of Results Presentation

This chapter discusses in detail the application of the models formulated above and compares with published experimental results. The pore size distribution is discussed as well as the effect of the progression of the dry-out zone on injectivity loss. The impact of salt precipitation on the reservoir rock properties such as porosity and permeability is also discussed.

4.2 Pore-Size Distribution

The pore size distribution gives a quantitative description of the range of pore sizes present in each core sample. In this study, the pore size distribution of a Berea sandstone was adopted and modelled as a bundle of parallel tubes, as already described in section 3.2. Typically, the spread of the pore sizes in a Berea sandstone is described by a log-normal distribution as shown on Figure 4.1. A variable r (radius of capillary tubes) has a log-normal distribution if $\log(r)$ is normally distributed. The probability density function for the log-normal distribution is given as:

$$P(r_t) = \frac{1}{x\sigma\sqrt{2\pi}} exp\left[-\frac{(\log(r_t) - \mu)^2}{2\sigma^2}\right] \tag{4.1}$$

where the variable r_t, is the radius of a single tube, randomly generated from a log-normal distribution with a mean, μ , standard deviation, σ and sample size of N which is the number of tubes in the core as computed from equation 3.32, using the PYTHON code attached in the appendix 5.2. The total number of tubes calculated is $1,391,126$ but for the sake of computational time, this value was reduced to $50,000$ tubes. The number of tubes give accuracy and a broader range

of tubes for investigations but reducing the number to a reasonable value does not really affect the results, as the general principles of the results are maintained. The mean and standard deviation are expressed respectively as;

$$\mu = \log\left(\frac{m}{\sqrt{1+\frac{v}{m^2}}}\right) \tag{4.2}$$

$$\sigma = \sqrt{\log\left(1+\frac{v}{m^2}\right)} \tag{4.3}$$

where, m and v are the non-logarithmized mean and variance respectively. The value for m is estimated as 1.0 for a Berea sandstone core whiles v is estimated to be 0.5.

Figure 4.1 shows the log-normal probability density function (PDF) of the tube radii. A high percentage of the tubes are very small pore channels within the size range of 0–20 μm, with the mode of the distribution being around 5 μm. The tube sizes within this range are modelled as pore throats where salt precipitation will likely occur whilst tube sizes above 20 μm are seen as pore bodies. A pore body will have about 4–5 pore throats connected to it and this exlains why there are many smaller tubes than larger ones in the diagram in Figure 4.1. It was modeled this way to achieve a cordination number similar to sandstones as the experimental data used in some part of this work is based on berea sandstone cores. Since we are using a bundle of tubes, the pores are seen as cappillary tubes. Salt precipitating in the smaller or larger pores will normally be difficult to predict. But since larger pores drain at lower entry pressures than smaller pores, and evaporation increases the concentration inside the pores, salt is more likely to precipitate in the smaller pores [51].

4.3 Effect of Dry-out Zone on Development of CO_2 Injectivity

The dry-out coefficient indicates the progression of the dry-out zone in a cylindrical core and thus the fraction of the core contaminated with precipitated salt. Salt precipitation occurs in the dry-out zone where most of the irreducible water in the trapped brine have evaporated leaving a high saturation of salt in that region. The precipitated salt accumulates in this dry-out zone impairing the flow channels which adversely affects injectivity. The extent and area of accumulation of the precipitated salt has been a subject of dispute amongst various published works. In the work of Roels [50], they suggested that the local salt accumulation in the field may occur far from the injection well where the flow velocities are much smaller, whereas Pruess [49] and Bacci et al. [3] indicated otherwise. Their

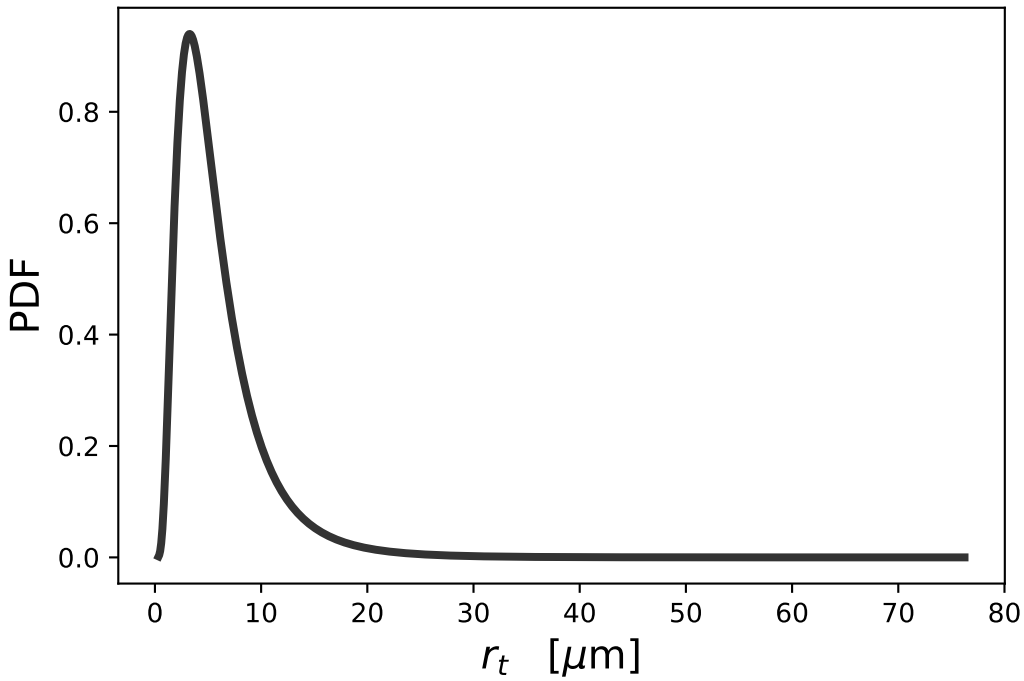

Figure 4.1: Log-normal probability distribution function (PDF) of tube radii

studies showed that the local salt accumulation occur in the near wellbore area where gas velocity is high. From Figure 4.2, our work seems to agree with the argument that the local salt accumulation occurs predominantly in the near wellbore region. The simulation results fit almost perfectly to measured data obtained from experimental results. We see from the figure that at a dryness coefficient of about 0.1, the injectivity is greatly reduced with a relative injectivity change of about 45 %. A relative injectivity change of 100 % signifies complete plugging of the core due to salt precipitation whiles 0 % signifies no precipitation of salt. Increase in α results in lower injectivity change and becomes almost constant between 0.4 to 0.8. This gives the indication that the local accumulation of precipitated salt occurs significantly at the region closer to the injection point. This could be explained by the action of capillary backflow. As the dry-out region progresses towards the interior of the core, precipitation begins at the injection point, making this area very high in salt concentration at any point in time along the length of the core. The precipitated salt has a significant affinity towards brine water and can imbibe the water from the displacement front across a concentration gradient–towards the injection area. Evaporation of the back-flowed brine leads to further salt accumulation. The accumulation therefore builds from the injection point and decreases towards the exit of the core.

At α values above 0.8, a little increase in injectivity loss is observed. This could be as a result of salt redistribution within the core. Continuous injection of gas after all the brine has been pushed out could redistribute the already precipitated

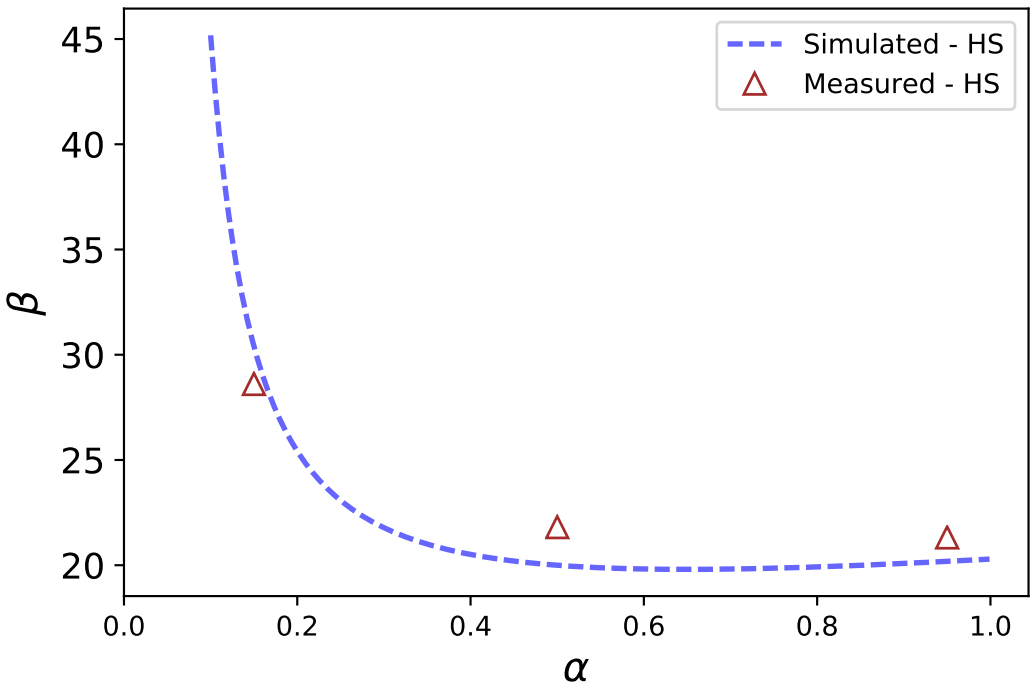

Figure 4.2: Dry-out coefficient vs relative injectivity change for simulated and experimental data

salt in the core which could possibly account for that observation.

The core flooding experiment of Andre et al. [1] showed a similar trend of salt accumulation. The precipitated salt accumulated only in the first 5 mm of the core in their experiment although the dry-out region had extended to the interior of the core. Miri and Hellevang [37] explained that, this occurs due to strong salt capillary suction and with a self-enhancing mechanism. These two physical mechanisms contributing to the process of salt precipitation have been explained in section 2.3 of this report.

Miri and Hellevang [37] further explained that the apparent disagreement on the location of salt accumulation could be that;

1. if the injection is within capillary drying regime, massive pore clogging will likely occur in the near well zone.

2. if the injection is within diffusive or evaporative drying regimes the precipitation will be less concentrated.

4.4 Effect of Brine Salinity

Brine salinity is one of the most important parameters that affects salt precipitation. From Figure 4.3, the effect of varying brine salinity is shown. The blue dashed line represents a case of high brine salinity of $1.148\,75\,\mathrm{g\,cm^{-3}}$, and the red line, a case of $1.0974\,\mathrm{g\,cm^{-3}}$ brine salinity. The model developed fits the experimental data perfectively for the different the brine salinities. It is broadly accepted in literature that higher salinity gives rise to higher amounts of salt precipitation and therefore leads to higher porosity reduction and effectively, injectivity impairment [37, 72, 42]. High salinity brine reaches and exceeds it solubility limit much faster, owing to evaporation of water into the gas phase. This leads to faster rate of precipitation and high accumulation of salt. In the works of Sokama-Neuyam and Ursin [57], they observed that, irrespective of the initial saturating brine salinity, salt precipitation could impair CO_2 injectivity. There have however not been proven results to ascertain a salinity envelope or limits above or below which the salinity of brine could be described as potentially harmful to injectivity. Such a finding will have to be dependent on prevailing subsurface and injection conditions such as formation and injection temperatures, injection pressure and rate, in situ mineral composition etc. These parameters will in one way of the other cause a shift the salinity envelope.

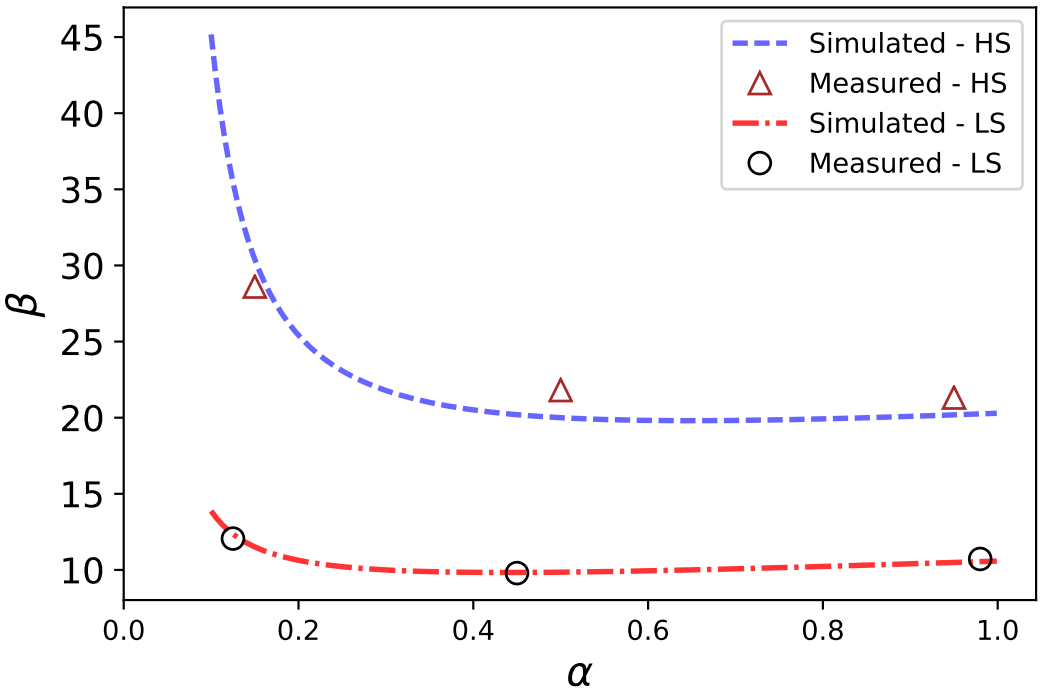

Figure 4.3: Effect of brine salinity on injectivity (HS-high salinity: $1.148\,75\,\mathrm{g\,cm^{-3}}$; LS-low salinity: $1.0974\,\mathrm{g\,cm^{-3}}$)

4.5 Porosity, Permeability and Solid Salt Interrelation

4.5.1 Porosity and Permeability Ratio

The direct effect of salt precipitation is the reduction in pore volume and permeability impairment since precipitated salt blocks pore throats and occupies a fraction of the pore space. Once the pore throats, which serve to connect the various pore spaces are reduced, fluid movement in the formation is greatly affected. Equation 4.4 by Verma and Pruess [65] was used to describe the effect of salt precipitation on permeability, where k_o and ϕ_o are the initial permeability and porosity respectively, before salt precipitation and k and ϕ are the permeability the porosity after salt precipitation.

$$\frac{k}{k_o} = \left(\frac{\phi}{\phi_o}\right)^3 \left(\frac{1-\phi_o}{1-\phi}\right)^2 \tag{4.4}$$

Equation 4.4 is a consequence of the Kozeny–Carman grain model and it does not have a direct inclusion of the salt saturation. A model for estimating reduction in porosity due to salt precipitation was proposed by Bolton et al. [6] as follows;

$$\phi = \phi_o \left(1 - S_s\right) \tag{4.5}$$

Combining equations 4.4 and 4.5 results in the 4.6 which expresses the permeability ratio as a function of initial porosity and solid salt saturation. This gives us the luxury to study the permeability ratio by varying the salt saturation, or other parameters affecting salt saturation.

$$\frac{k}{k_o} = (1 - S_s)\left(\frac{1-\phi_o}{1-\phi_o(1-S_s)}\right)^2 \tag{4.6}$$

Figure 4.4 shows a plot of the permeability ratio versus porosity ratio. From this, we see a rapid decline in permeability as against porosity. Permeability essentially is concerned with the conductance of fluid in porous media and all it takes for the reduction in permeability of the formation is for the precipitated salt to block the pore throats. These pore throats enhance connectivity between the pores in the formation allowing fluid flow. Porosity on the other hand is about the capacity of the reservoir rock volume to hold fluid; it is just a fraction of the void volume in the rock. For porosity to become zero will mean a total collapse of all the void spaces, which in our case will mean total filling of the void spaces with accumulated salt. This is a highly unlikely event. If we compare the mechanisms for permeability impairment (pore throat blocking) and porosity reduction (pore volume reduction) owing to precipitated salt, then it is likely that permeability impairment will be

affected the more and we see this on Figure 4.4. On the extreme scenario, it makes sense to have a porous but impermeable rock, than a permeable rock with no porosity. On Figure 4.4, core drying experiments performed by Bacci et al. [3] is also plotted. Their results fit our model quite well and as presented in Table 4.1, they recorded high percentage reduction in permeability for each drying process than porosity reduction.

Table 4.1: Porosity and permeability measurements during salt precipitation [3]

	Porosity (%)	**Porosity reduction (%)**	**Permeability (md)**	**Permeability reduction (%)**
Un-altered sample	22.59	0	7.78	0
After first vaporisation test	21.58	4.47	5.39	30.72
After second vaporisation test	19.44	13.94	2.96	59.77
After third vaporisation test	18.27	19.12	2.57	66.97
After forth vaporisation test	15.10	29.08	1.07	86.25

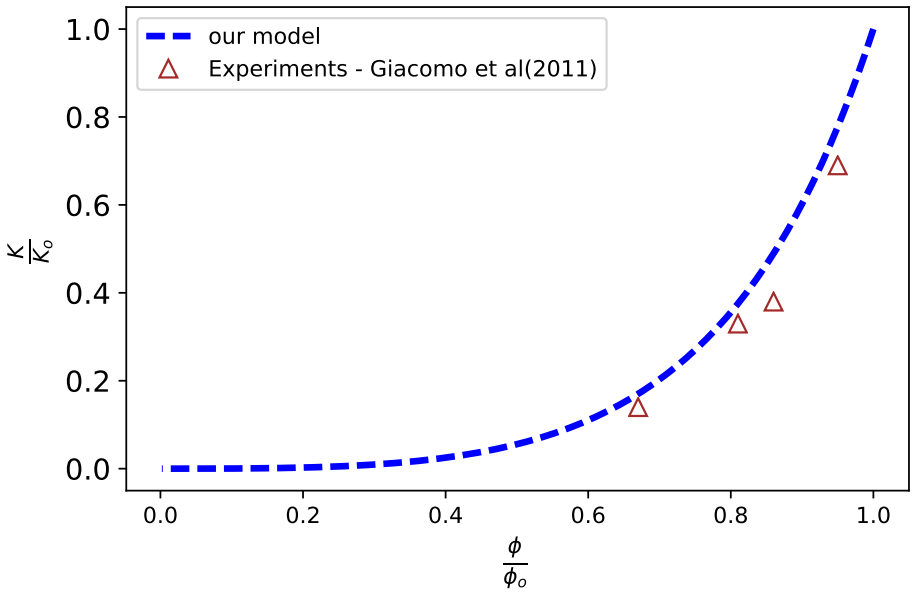

Figure 4.4: Effect of salt precipitation on permeability and porosity relationship

4.5.2 Effect of Initial Permeability

At a solid salt saturation of 0.0, the permeability remains as the initial. Once precipitation starts and salt accumulation begins, the permeability begins to reduce significantly, thus assuming no other permeability reduction process is taking place. After a certain salt saturation, the rate of permeability reduction slows down as can be seen on Figure 4.5. At this point, it could be that, precipitation is occurring at a relatively slower rate due to all the brine being pushed out of the core. The slow rate of precipitation could also be that, less brine water is evaporating into the gas phase making it difficult to reach the solubility limit of the salt below which the salt will form. In situations where the relative distance between the displacement front and the drying front is wide, precipitation resulting from capillary backflow could reduce due to reduced effect of the already precipitated salt concentration to draw brine water over the distance.

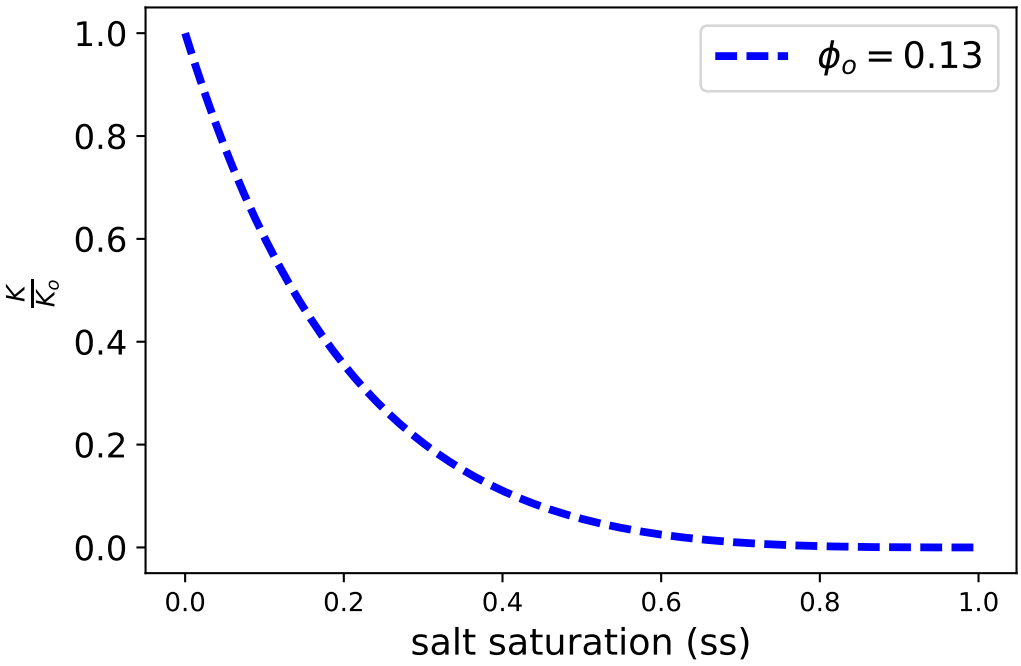

Figure 4.5: Effect of salt precipitation on permeability

4.5.3 Effect of Initial Porosity on Permeability Alteration

In Figure 4.6, a sensitivity on the effect of salt saturation on permeability ratio with varying initial porosity is shown. At a high porosity of 65 %, the permeability reduction occurs more rapidly than for low porosities (30 % and and 13 %). One would have expected the opposite to be the case as fewer pores will easily get plugged by salt. But this could be that high porosity rocks retains more brine, precipitating more salts per given time.

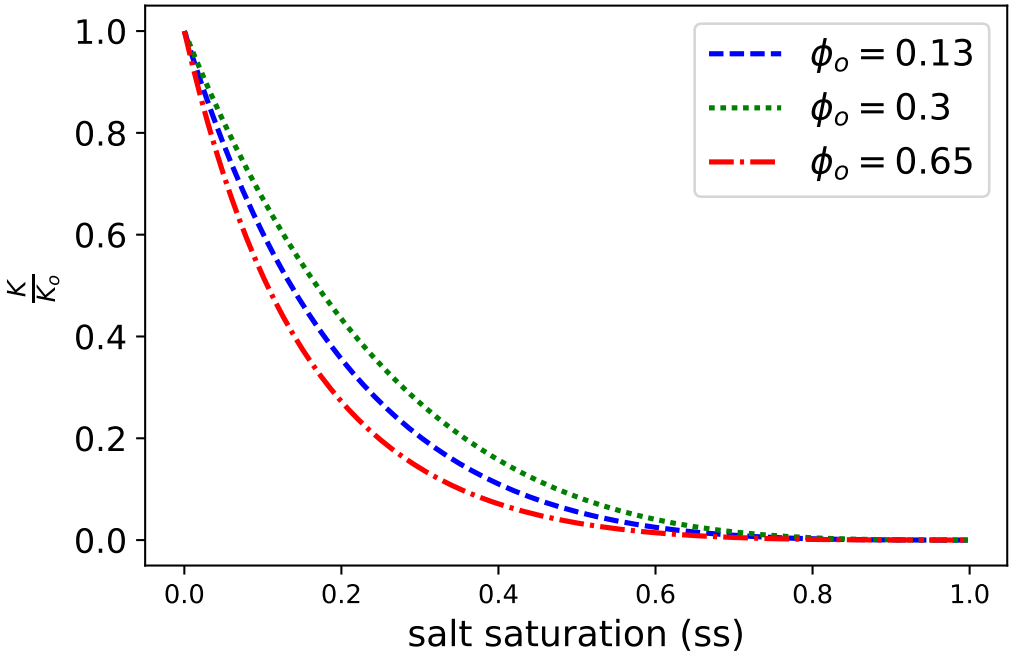

Figure 4.6: Permeability alteration as a function of salt saturation showing effect of varying initial porosity

4.5.4 Effect of Initial Permeability on Salt Saturation

On Figure 4.7, three cases of initial permeability were investigated and are shown. It can be observed that the initial permeability of the reservoir rock has a big impact on the salt precipitation profile. In rocks with high initial permeability, salt precipitation is minimal. High permeability favours faster fluid transport, and as such, there is less brine hold-up the reservoir rock which will be exposed to the injected gas and evaporate the brine water. Unlike high permeability rocks, low permeability rocks retain more brine at any position at any given time precipitating more salts. Roels [50] explained in their experimental work that, in low permeability sandstone cores, the narrow pore throats, delay brine breakthrough and favour precipitation of minerals.

4.6 Effect of Injection Flow Rate

Generally, increasing injection flowrate leads to increase in pressure loss across a core sample as is evident from equation 3.20. This equation can be rewritten in terms of injection flowrate as;

$$\Delta p = Q \times \frac{1}{I_f} \tag{4.7}$$

where $\frac{1}{I_f}$ is the slope of the equation and equals the inverse of the injectivity

reduction (final injectivity) resulting from salt precipitation. I_f is a function of solid salt saturation, which in turn depends on salinity as derived in equation 3.45. On Figure 4.8 the pressure drop is plotted against the injection flowrate, for two different brine salinities. A case of no brine salinity, which in a way represents fresh water is also plotted as the black curve. It is assumed that, since no salinity is present in this case, there will be no salt precipitation.

The pressure drop for the case with both low and high salinities can be rewritten from equation 3.19 as:

$$\Delta P = \frac{Q}{\frac{\pi}{8\mu\tau L}\sum_{i=1}^{N}\left[\frac{1}{\frac{\alpha}{(r_i-\Delta r_i)^4}+\frac{1-\alpha}{r_i^4}}\right]} \tag{4.8}$$

For the case with no salinity, equation 4.8 reduces to

$$\Delta P = \frac{Q}{\frac{\pi}{8\mu\tau L}\sum_{i=1}^{N} r_i^4} \tag{4.9}$$

with similar assumptions as applied to equation 3.23.

The values of injection flowrate, Q, used in this study, ranged between $1ml/min$ to $10ml/min$. These values were chosen based on similar values used for earlier experimental studies at UiS by Sokama-Neuyam and Ursin [57]. At very low

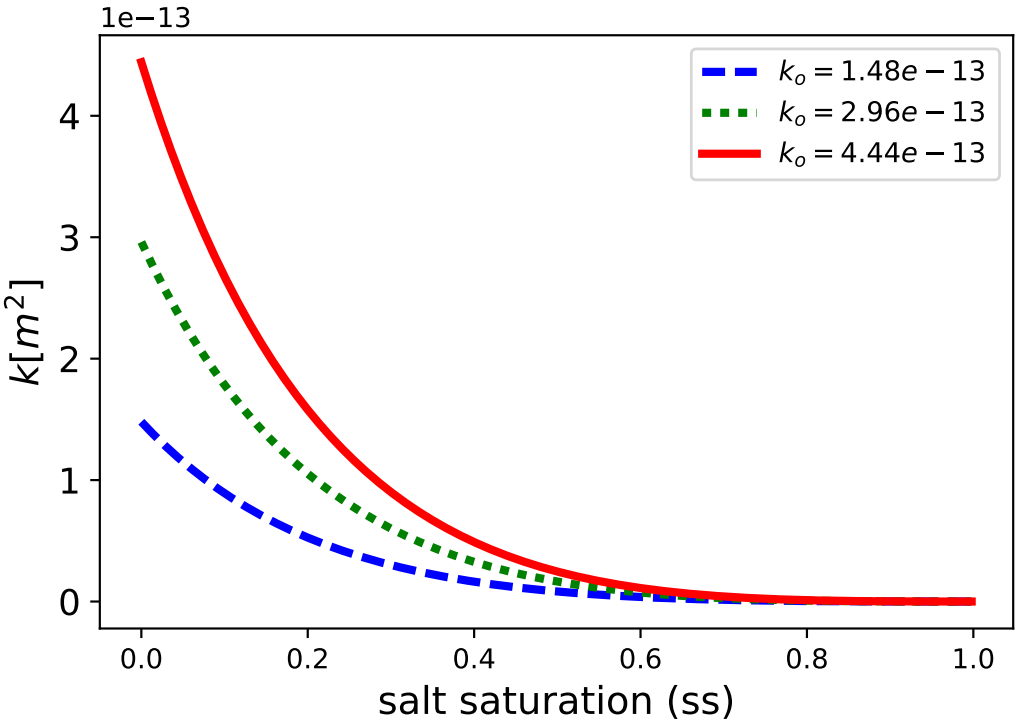

Figure 4.7: Permeability variation as a function of salt saturation for three different initial permeabilitys. (red=150md, green=300md, blue=450md)

injection flowrates, the pressure drop is almost similar for the three cases of brine salinities (Figure 4.8). This gives the indication that, salinity may not be that important at low injection rates. With increase in the flowrate however, a clear difference between the three curves is seen. Pressure drop becomes highest in the case of high salinity and lowest when salinity was zero. The precipitated salt, whose degree of accumulation depends on salinity as already discussed under section 4.4, acts as a barrier that hampers the propagation of CO_2 and adds an extra pressure drop component which results in the high overall pressure drop.

The equations of the three lines are given by:

1. **Case 1:**no salinity: (No precipitation)

$$\Delta P = 47.63x \tag{4.10}$$

2. **Case 2:**low salinity: (precipitation)

$$\Delta P = 52.37x \tag{4.11}$$

3. **Case 3:** high salinity: (precipitation)

$$\Delta P = 60.298x \tag{4.12}$$

The reduction in injectivity can be inferred from the inverse of the slopes of these equations, with case 1 being our base case. By base case we mean, no permeability impairment and no injectivity reduction resulting from precipitated salt. The average Injectivity for **case 1** is $\frac{1}{47.634}$, which equals $0.021\,\mathrm{mL\,bar^{-1}\,min^{-1}}$. Similarly, the injectivity for **cases 2** and **3** are 0.0190 and $0.0166\,\mathrm{mL\,bar^{-1}\,min^{-1}}$ respectively. From these we see that the injectivity reduction is highest for case 3 with high salinity. The relative injectivity change, β, is 20.95%. For Case 2 with low salinity, β is 9.52%. This shows the adverse effects of salt precipitation and the significant role salinity plays in salt precipitation. High flowrates induce high salt precipitation which causes an appreciable pressure build-up, which decreases injectivity.

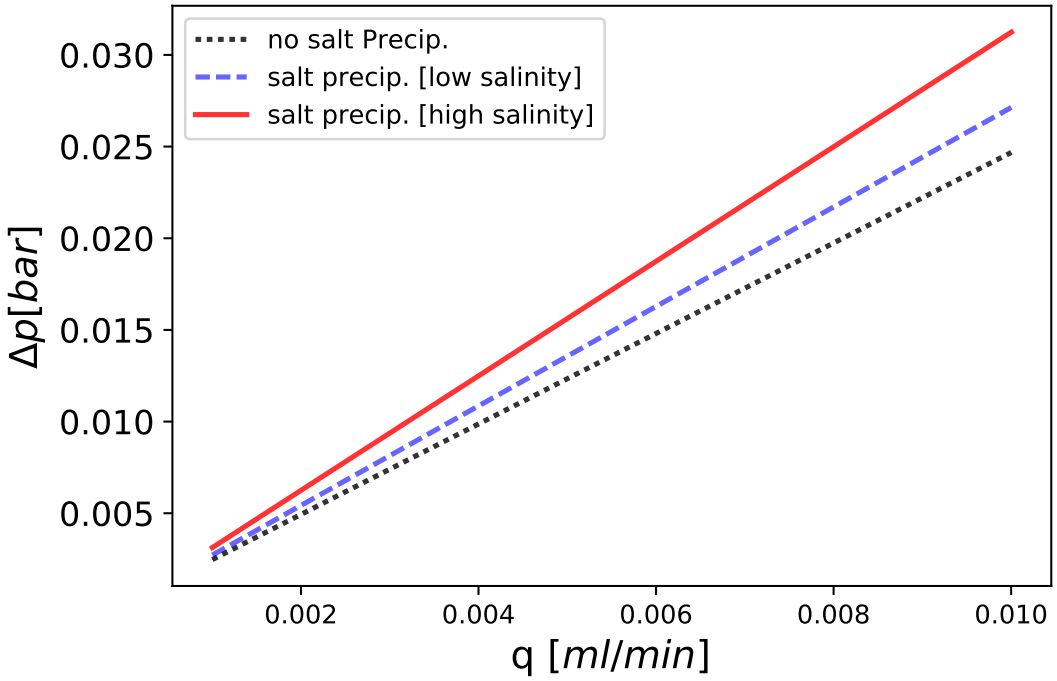

Figure 4.8: Pressure drop as a function of Injection flowrate for varying brine salinity

Chapter 5

Conclusion

5.1 Summary and Highlights

This research work has presented a simple theoretical model to quantify injectivity loss resulting from salt precipitation during the injection of supercritical CO_2 into saline aquifers. The model was developed using a bundle of tubes and it assumed no compressibility, no temperature and pressure effects, non-reactive rock and other simplying assumptions.

A sensitivity study performed to assess the effects of parameters such as salinity, initial permeability, injection flowrate and porosity on injectivity loss led to the following general observations;

1. Salt precipitation occurs in the dry-out zone where most of the irreducible water in the trapped brine have evaporated leaving a high saturation of salt in that region but salt accumulation occur predominantly closer to the injection point. Figure 4.2.

2. Increasing brine salinity has adverse effects on injectivity. This is a widely accepted phenomenom in literature and the present model agrees with that. Figure 4.3.

3. Salt precipitation affects permeability of porous media more than it affects porosity. Permeability essentially is concerned with the conductance of fluid in porous media and the blocking of pore throats by the precipitated salt reduces perameability. Porosity on the other hand defines the capacity of the reservoir rock volume to hold fluid. Reduction of porosity to zero will mean total filling of the void spaces with precipitaed salt—a highly unlikely event compared with permeability reduction by pore throat blocking. Figure 4.4

4. Rock Peameability reduces faster at even lower salt saturations but the rate of reduction slows down with increasing salt saturation. Figure 4.5

5. At a high porosity (65%), the permeability reduction occurs more rapidly than for low porosities (30% and 13%). High porosity rocks retains more brine, precipitating more salts per given time. Figure 4.6

6. In rocks with high initial permeability, salt precipitation is minimal. High permeability favours faster fluid transport, and as such, there is less brine hold-up in the porous medium which will be exposed to the injected CO_2 to evaporate the brine water. Figure 4.6

7. High flowrates induce high salt precipitation which causes an appreciable pressure build-up. This oberservation however conflicts most works conducted by other researchers. Figure 4.8

In summary, for the range of parameters studied, the results suggest that salt precipitation poses a threat to CO_2 sequestration in saline aquifers. Although this work made use of many assumptions for simplicity, the findings are important for understanding the basic effect of salt precipitation on CO_2 injectivity.

5.2 Further Work

Moving forward, the following can be considered for improved understanding of injectivity loss resulting from salt precipitation;

1. Modelling the effect of temperature will be essential in understanding more of the subsurface mechanisms. The injected gas and aquifer have different temperatures.

2. The present model is basically for the quantification of injectivity loss. A study to incorporate the effect of relative permeability of both the gaseous and aqueous phases and also hysteris will be essential.

3. A more representative pore scale model other than the bundle of tubes could be considered also.

4. The current study also ignored kinetic and frictional pressure losses which may be important for subsurface fluid flow due to density variation and irregular flow channels. Incoporaration of these will be important.

Bibliography

[1] Laurent Andre, Yannick Peysson, and Mohamed Azaroual. "Well injectivity during CO2 storage operations in deep saline aquifers–Part 2: Numerical simulations of drying, salt deposit mechanisms and role of capillary forces". In: *international journal of Greenhouse Gas Control* 22 (2014), pp. 301–312.

[2] David Archer. "Fate of fossil fuel CO2 in geologic time". In: *Journal of Geophysical Research: Oceans* 110.C9 (2005).

[3] Giacomo Bacci, Anna Korre, and Sevket Durucan. "Experimental investigation into salt precipitation during CO2 injection in saline aquifers". In: *Energy Procedia* 4 (2011), pp. 4450–4456.

[4] Abhoyjit S Bhown and Brice C Freeman. "Analysis and status of post-combustion carbon dioxide capture technologies". In: *Environmental science & technology* 45.20 (2011), pp. 8624–8632.

[5] Martin J Blunt, Branko Bijeljic, Hu Dong, Oussama Gharbi, Stefan Iglauer, Peyman Mostaghimi, Adriana Paluszny, and Christopher Pentland. "Pore-scale imaging and modelling". In: *Advances in Water Resources* 51 (2013), pp. 197–216.

[6] Edward W Bolton, Antonio C Lasaga, and Danny M Rye. "Long-term flow/chemistry feedback in a porous medium with heterogenous permeability; kinetic control of dissolution and precipitation". In: *American Journal of Science* 299.1 (1999), pp. 1–68.

[7] Se E Buckley, MCi Leverett, et al. "Mechanism of fluid displacement in sands". In: *Transactions of the AIME* 146.01 (1942), pp. 107–116.

[8] Michael A Celia and Jan M Nordbotten. "Practical modeling approaches for geological storage of carbon dioxide". In: *Groundwater* 47.5 (2009), pp. 627–638.

[9] Organisation Internationale des Constructeurs d'Automobiles (OICA). *Climate Change & CO2*. accessed 22-May-2017. URL: http://www.oica.net/category/climate-change-and-co2/.

[10] Helge K Dahle, Michael A Celia, and S Majid Hassanizadeh. "Bundle-of-tubes model for calculating dynamic effects in the capillary-pressure-saturation relationship". In: *Upscaling Multiphase Flow in Porous Media*. Springer, 2005, pp. 5–22.

[11] MMI Al-Doury. "A Discussion About Hydraulic Permeability and Permeability". In: *Petroleum Science and Technology* 28.17 (2010), pp. 1740–1749.

[12] EU. *What is climate change?* accessed 23-May-2017. Dec. 2011. URL: https://ec.europa.eu/clima/sites/campaign/what/climatechange_en.htm.

[13] Irving Fatt et al. "The network model of porous media". In: *One Petro* (1956).

[14] Darryl H Fenwick and Martin J Blunt. "Three-dimensional modeling of three phase imbibition and drainage". In: *Advances in Water Resources* 21.2 (1998), pp. 121–143.

[15] Darryl H Fenwick, Martin J Blunt, et al. "Network modeling of three-phase flow in porous media". In: *SPE Journal* 3.01 (1998), pp. 86–96.

[16] José D Figueroa, Timothy Fout, Sean Plasynski, Howard McIlvried, and Rameshwar D Srivastava. "Advances in CO2 capture technology—the US Department of Energy's Carbon Sequestration Program". In: *International journal of greenhouse gas control* 2.1 (2008), pp. 9–20.

[17] Sarah M Forbes, Preeti Verma, Thomas E Curry, S Julio Friedmann, Sarah M Wade, et al. "Guidelines for carbon dioxide capture, transport and storage." In: *Guidelines for carbon dioxide capture, transport and storage.* (2008).

[18] Thomas Giorgis, Michele Carpita, and Alfredo Battistelli. "2D modeling of salt precipitation during the injection of dry CO2 in a depleted gas reservoir". In: *Energy Conversion and Management* 48.6 (2007), pp. 1816–1826.

[19] Mary Griffiths, Paul Cobb, and J Marr-Laing. "Carbon Capture and Storage: An arrow in the quiver or a silver bullet to combat climate change". In: *A Canadian Primer. The Pembina Institute. Retrieved February* 13 (2005), p. 2008.

[20] T.M. Halmø. *The Gas Value Chain: Compendium PET 545*. Spring Term. University of Stavanger. 2016.

[21] DL Hartmann, AMG Klein Tank, Matilde Rusticucci, LV Alexander, Stefan Brönnimann, Y Charabi, FJ Dentener, EJ Dlugokencky, DR Easterling, Alexey Kaplan, et al. "Observations: atmosphere and surface". In: (2013).

[22] AA Heiba, HT Davis, LE Scriven, et al. "Statistical network theory of three-phase relative permeabilities". In: *SPE Enhanced Oil Recovery Symposium*. Society of Petroleum Engineers. 1984.

[23] Suzanne Hurter, Johan Gerhard Berge, Diane Labregere, et al. "Simulations for CO2 injection projects with compositional simulator". In: *Offshore Europe*. Society of Petroleum Engineers. 2007.

[24] What's Your Impact. *Main sources of carbon dioxide emissions*. accessed 22-May-2017. n.d. URL: http://whatsyourimpact.org/greenhouse-gases/carbon-dioxide-emissions.

[25] *In Salah CO2 Storage*. accessed 22-May-2017. Dec. 2015. URL: http://www.globalccsinstitute.com/projects/salah-co2-storage.

[26] Louis-Marie Jacquelin. *Public Acceptance Problematic*. accessed 16-May-2017. Nov. 2010. URL: http://www.globalccsinstitute.com/insights/authors/louis-mariejacquelin/2010/11/05.

[27] Li Jian-Hua and Yu Bo-Ming. "Tortuosity of flow paths through a Sierpinski carpet". In: *Chinese Physics Letters* 28.3 (2011), p. 034701.

[28] Kim Johnsen, Kaare Helle, Sigbjørn Røneid, and Hamish Holt. "DNV recommended practice: Design and operation of CO2 pipelines". In: *Energy Procedia* 4 (2011), pp. 3032–3039.

[29] JR Kelafant, SH Stevens, and CM Boyer. "Vast resource potential exists in many countries". In: *Oil and Gas Journal;(United States)* 90.44 (1992).

[30] Helge Kongsjorden, Olav Kårstad, and Tore A Torp. "Saline aquifer storage of carbon dioxide in the Sleipner project". In: *Waste management* 17.5-6 (1998), pp. 303–308.

[31] A Koponen, M Kataja, and Jv Timonen. "Tortuous flow in porous media". In: *Physical Review E* 54.1 (1996), p. 406.

[32] Andrew A Lacis, Gavin A Schmidt, David Rind, and Reto A Ruedy. "Atmospheric CO2: Principal control knob governing Earth's temperature". In: *Science* 330.6002 (2010), pp. 356–359.

[33] *Large-scale CCS facilities*. accessed 5-June-2017. n.d. URL: http://www.globalccsinstitute.com/projects/large-scale-ccs-projects.

[34] Dennis YC Leung, Giorgio Caramanna, and M Mercedes Maroto-Valer. "An overview of current status of carbon dioxide capture and storage technologies". In: *Renewable and Sustainable Energy Reviews* 39 (2014), pp. 426–443.

[35] Bert Metz, Ogunlade Davidson, Heleen De Coninck, Manuela Loos, and Leo Meyer. *IPCC special report on carbon dioxide capture and storage*. Tech. rep. Intergovernmental Panel on Climate Change, Geneva (Switzerland). Working Group III, 2005.

[36] Rohaldin Miri. "Effects of CO2 -Brine-Rock Interactions on CO2 Injectivity – Implications for CCS". PhD thesis. University of Oslo, 2015.

[37] Rohaldin Miri and Helge Hellevang. "Salt precipitation during CO2 storage—A review". In: *International Journal of Greenhouse Gas Control* 51 (2016), pp. 136–147.

[38] SG Mohammed. "Dynamic Pore-Scale modelling of Two-Phase flow". PhD thesis. Dissertation of Doctoral Degree. London: Imperial College, 2004 Google Scholar, 2004.

[39] Nadja Muller, Ran Qi, Elizabeth Mackie, Karsten Pruess, and Martin J Blunt. "CO2 injection impairment due to halite precipitation". In: *Energy procedia* 1.1 (2009), pp. 3507–3514.

[40] Hiroki Muroyama, Yuji Tsuda, Toshiki Asakoshi, Hasan Masitah, Takeou Okanishi, Toshiaki Matsui, and Koichi Eguchi. "Carbon dioxide methanation over Ni catalysts supported on various metal oxides". In: *Journal of Catalysis* 343 (2016), pp. 178–184.

[41] Gautam Naik. *Slowdown in Warming Tied to Less Water Vapor*. accessed 22-May-2017. Jan. 2010. URL: https://www.wsj.com/articles/SB10001424052748704194504575031404275769886.

[42] Rohith Nair. *Near Wellbore Salt Precipitation in Gas Reservoirs*. 2015.

[43] NASA. *A blanket around the Earth*. accessed 16-May-2017. 2014. URL: https://climate.nasa.gov/causes/.

[44] Mihaela Norişor, Adrian Badea, and Cristian Dincă. "Economical and technical analysis of CO2 transport ways". In: *UPB Sci Bull* 74.1 (2012), pp. 303–308.

[45] Abass A Olajire. "A review of mineral carbonation technology in sequestration of CO2". In: *Journal of Petroleum Science and Engineering* 109 (2013), pp. 364–392.

[46] Dani Or and Markus Tuller. "Flow in unsaturated fractured porous media: Hydraulic conductivity of rough surfaces". In: *Water Resources Research* 36.5 (2000), pp. 1165–1177.

[47] H Ott, SM Roels, and K De Kloe. "Salt precipitation due to supercritical gas injection: I. Capillary-driven flow in unimodal sandstone". In: *International Journal of Greenhouse Gas Control* 43 (2015), pp. 247–255.

[48] Mohammad Piri. "Pore-scale modelling of three-phase flow". PhD thesis. Imperial College, 2003.

[49] Karsten Pruess. "Formation dry-out from CO2 injection into saline aquifers: 2. Analytical model for salt precipitation". In: *Water Resources Research* 45.3 (2009).

[50] Saskia Maria Roels. *Formation dry-out and injectivity impairment during CO2 storage in saline aquifers*. Vol. 2. Research conducted as part of the Dutch National Program of CCS: CATO-2, 2015.

[51] George W Scherer. "Stress from crystallization of salt". In: *Cement and concrete research* 34.9 (2004), pp. 1613–1624.

[52] Australian Academy of Science. *The science of climate change: Questions and answers*. accessed 22-May-2017. Feb. 2015. URL: www.science.org.au/climatechange.

[53] Brad A Seibel and Patrick J Walsh. "Potential impacts of CO2 injection on deep-sea biota". In: *Science* 294.5541 (2001), pp. 319–320.

[54] JQ Shi and S Durucan. "CO2 storage in deep unminable coal seams". In: *Oil & gas science and technology* 60.3 (2005), pp. 547–558.

[55] Keith P Shine and Ashok Sinha. "Sensitivity of the Earth's climate to height-dependent changes in the water vapour mixing ratio". In: *Nature* 354.6352 (1991), p. 382.

[56] The Royal Society and the US National Academy of Sciences. *Climate Change: Evidence & Causes*. nd. URL: https://nas-sites.org/americasclimatechoices/more-resources-on-climate-change/climate-change-%20evidence-and-causes/.

[57] Yen Adams Sokama-Neuyam and Jann Rune Ursin. "Experimental and theoretical investigations of CO2 injectivity". In: *AGH Drilling, Oil, Gas* 33 (2016).

[58] WE Soll and MA Celia. "A modified percolation approach to simulating three-fluid capillary pressure-saturation relationships". In: *Advances in Water Resources* 16.2 (1993), pp. 107–126.

[59] Nicolas Spycher and Karsten Pruess. "CO2-H2O mixtures in the geological sequestration of CO2. II. Partitioning in chloride brines at 12–100 C and up to 600 bar". In: *Geochimica et Cosmochimica Acta* 69.13 (2005), pp. 3309–3320.

[60] Michael Sterner. *Bioenergy and renewable power methane in integrated 100% renewable energy systems: Limiting global warming by transforming energy systems*. Vol. 14. kassel university press GmbH, 2009.

[61] Rickard Svensson, Mikael Odenberger, Filip Johnsson, and Lars Strömberg. "Transportation systems for CO2—-application to carbon capture and storage". In: *Energy conversion and management* 45.15 (2004), pp. 2343–2353.

[62] Junwang Tang, Zhengxia Guo, and Afson Jamali. *CO2 capture and photocatalytic conversion to a renewable fuel on nanostructured catalysts*. accessed 16-May-2017. 2008. URL: http://www.ucl.ac.uk/btg/FeedbackReports/BtGReportTang1.html.

[63] Yong Tang, Ruizhi Yang, Zhimin Du, and Fanhua Zeng. "Experimental study of formation damage caused by complete water vaporization and salt precipitation in sandstone reservoirs". In: *Transport in Porous Media* 107.1 (2015), pp. 205–218.

[64] *Technology Roadmap: Carbon capture and storage*. Tech. rep. International Energy Agency, 2013.

[65] A Verma and K Pruess. "Thermohydrological conditions and silica redistribution near high-level nuclear wastes emplaced in saturated geological formations". In: *Journal of Geophysical Research: Solid Earth* 93.B2 (1988), pp. 1159–1173.

[66] Herausgegeben von. "Renewable Energies and Energy Efficiency". PhD thesis. Universität Kassel, Sept. 2009.

[67] Lasse Wallquist, Selma L'Orange Seigo, Vivianne HM Visschers, and Michael Siegrist. "Public acceptance of CCS system elements: a conjoint measurement". In: *International Journal of Greenhouse Gas Control* 6 (2012), pp. 77–83.

[68] DJ Wuebbles, AK Jain, KO Patten, and KE Grant. "Sensitivity of direct global warming potentials to key uncertainties". In: *Climatic Change* 29.3 (1995), pp. 265–297.

[69] Qingrong Xiong, Todor G Baychev, and Andrey P Jivkov. "Review of pore network modelling of porous media: experimental characterisations, network constructions and applications to reactive transport". In: *Journal of Contaminant Hydrology* 192 (2016), pp. 101–117.

[70] Mohammad Abu Zahra. "CCS Status and Challenges to Large Scale Deployment". In: IEA Greenhouse Gas R&D Programme. Linde Group Workshop, Mar. 2010.

[71] Mehdi Zeidouni, Mehran Pooladi-Darvish, and David Keith. "Analytical solution to evaluate salt precipitation during CO2 injection in saline aquifers". In: *International Journal of Greenhouse Gas Control* 3.5 (2009), pp. 600–611.

[72] Mehdi Zeidouni, Mehran Pooladi-Darvish, and David Keith. "Sensitivity analysis of salt precipitation and CO2-brine displacement in saline aquifers". In: *SPE International Conference on CO2 Capture, Storage, and Utilization*. Society of Petroleum Engineers. 2009.

Appendix

PYTHON Code

```
import numpy as np
from matplotlib import pyplot as plt
import scipy as sp
import matplotlib

#=============================================================================
# # Estimate N, the average number of tubings in the core
#=============================================================================
poro_init = 0.184                              # Initial porosity
R = 3.81/200                                   # Core radius
tube_rad_avg = 6e-6                            # Average tube radius
N = int (3/4*poro_init*(R/tube_rad_avg)**2)#Number of tubes in core

##Tortuousity Models
Tg=1+0.8(1-poro_init)                                 #Kaponen et al (1996)
#Tg=(19/18)**np.log(poro_init)/np.log(8/9)   #Li and Yu(2010)
#Tg=poro_init**(-0.4)                                 #mota et al (2001)
#Tg=1-*0.49np.log(poro_init)                          #Pech (1984)

# Lognormal distribution of tubes in the core
length_core = 0.2                 # (L) length of core (m)
m = 1                               # mean value
v = 0.5                           # variance
mu = np.log((m**2)/np.sqrt(1+(v/m**2)))#myu for lognormal function
sigma = np.sqrt(np.log(v/(m**2)+1)) # sigma for lognormal function

def lognpdf(x,mean,sig):
        a    = 1./(x*sig*sp.sqrt(2*sp.pi))
        pdf =  a*sp.exp(-(sp.log(x)-mean)**2/(2.*sig**2))
        return pdf

rad_tube = np.random.lognormal(mu,sigma,50000)
rad_tube = np.sort(rad_tube)
P = lognpdf(rad_tube,mu,sigma)
```

```
rad_tube1 = rad_tube*tube_rad_avg
rad_tube2=rad_tube1

#=================================================================
#Estimating injectivity coefficient
#=================================================================
#experimental data
dry_coef = 0.05
D_aq = 1.0974
X_s = 0.07168
D_aq1 = 1.14875
X_s1 = 0.1369
D_s = 2.16

dry_coef1 = np.arange(0.1,1,0.001)

betadry=[]
betadry1=[]
#while dry_coef <= 1:

for m in dry_coef1:
    #salt_sat = (0.94 - m/10)*(D_aq*X_s/D_s)
    salt_sat = (0.85 + m/3.5)*(D_aq*X_s/D_s)
    del_r = (2/3)*(rad_tube1*salt_sat)/m
    diff = rad_tube1 - del_r
    I_i = np.sum(rad_tube1**4)
    I_f = np.sum((1/((m/(diff)**4)+((1-m)/rad_tube1**4))))
    beta = (1 - (I_f/I_i))*100
    betadry.append(beta)

for m in dry_coef1:
    #salt_sat = (0.94 - m/10)*(D_aq*X_s/D_s)
    salt_sat = (0.85 + m/3.5)*(D_aq1*X_s1/D_s)
    del_r = 2/3*(rad_tube1*salt_sat)/m
    diff = rad_tube1 - del_r
    I_i = np.sum(rad_tube1**4)
    I_f = np.sum((1/((m/(diff)**4)+((1-m)/rad_tube1**4))))
    beta = (1 - (I_f/I_i))*100
    betadry1.append(beta)
#=================================================================
#Figure plotting
#=================================================================
plt.figure(1)
plt.plot(dry_coef1,betadry1,"--", lw=2, color="blue", alpha=0.6,
         label='Simulated - HS')
plt.plot((0.15, 0.5,0.95), (28.61,21.81,21.32),'^',
```

```
81          ms=8, markerfacecolor= "None",
82         markeredgecolor='brown', markeredgewidth=1,
83         label='Measured - HS')
84
85 plt.plot(dry_coef1,betadry,"-", lw=2, color="red", alpha=0.8,
86         label='Simulated - LS')
87 plt.plot((0.125,0.45,0.98), (12.06,9.79,10.72),'o', ms=8,
88          markerfacecolor= "None",
89            markeredgecolor='black', markeredgewidth=1,
90            label='Measured - LS')
91
92 plt.legend()
93
94 plt.xticks(np.arange(min(dry_coef1)-0.1, max(dry_coef1)+0.1, 0.2))
95 plt.yticks(color='k', size=13)
96 plt.xlabel(r'$\alpha$',{'color': 'k','fontsize': 15})
97 plt.ylabel(r'$\beta$',{'color': 'k','fontsize': 15})
98
99 plt.savefig('Chart1_Bundle of tubes_2', format='png', dpi=1500)
100 plt.show()
101
102 plt.figure(2)
103 plt.plot(rad_tube1,P, lw=3, color="black", alpha=0.8,)
104 plt.xlabel(r'$r_t$',{'color': 'k','fontsize': 15})
105 plt.ylabel(r'PDF',{'color': 'k','fontsize': 15})
106
107 plt.savefig('pdf', format='png', dpi=1500)
108 plt.show()
109 #=============================================================
```